

UNIVERSIDADE DE LISBOA
Faculdade de Ciências
Departamento de Física



**Regional Quantification of Lung Function in Cystic Fibrosis
using hyperpolarized Xenon-129 and Chemical Shift Imaging**

Carolina Campanha Fernandes

Dissertação

Mestrado em Engenharia Biomédica e Biofísica
Radiações em Diagnóstico e Terapia

2012

UNIVERSIDADE DE LISBOA
Faculdade de Ciências
Departamento de Física



**Regional Quantification of Lung Function in Cystic Fibrosis
using hyperpolarized Xenon-129 and Chemical Shift Imaging**

Carolina Campanha Fernandes

Dissertação orientada pelos Prof. Doutores Jaime Mata e

Eduardo Ducla-Soares

Mestrado em Engenharia Biomédica e Biofísica

Radiações em Diagnóstico e Terapia

2012

Abstract

Cystic fibrosis (CF) is a genetic disorder in which the defective gene causes the production of unusually thick and viscous mucus that builds-up in the airways, leading to impaired ventilation and infection of lung structures. Currently, there is a lack of methods capable of routinely assessing, in a regional manner, basic physiological processes that occur in the lung, such as pulmonary gas uptake-exchange. The technique described in this study makes use of hyperpolarized Xenon-129 (HP Xe-129) gas and chemical shift imaging (CSI), for non-invasively obtaining three dimensional regional characterization of gas ventilation, and gas uptake-exchange in lung tissue and in red blood cells (RBC). Here the feasibility of this method is demonstrated for evaluating Xe-129 distribution in multiple lung compartments in subjects with CF and in healthy subjects.

CSI maps of HP Xe-129 as gas in the airspaces and dissolved in lung tissue and in the RBC were generated for each slice of each subject. The ratio of gas dissolved in the tissue to that dissolved in the RBC was also obtained, allowing us to infer about pulmonary membrane thickness.

The results demonstrated that healthy subjects presented uniform ventilation and gas uptake-exchange in the lung parenchyma and in the RBC. On the other hand, multiple regional defects were observed in all lung compartments in the CF population, indicating that current CSI map resolution is sufficient to detect focal disease. Xe-129 CSI quantification was capable of clearly distinguishing CF from healthy population. CF subjects presented a higher tissue/RBC ratio, probably due to inflammation of the lung tissue walls.

The preliminary data presented here let us hypothesize that this technique is able to provide, in a single short breath-hold, detailed physiological information, with potential to detect small changes in the progression of various pulmonary diseases.

Keywords: cystic fibrosis, hyperpolarized Xenon-129, chemical shift imaging, ventilation, gas uptake-exchange.

Resumo

Fibrose cística é a doença hereditária mais comum e fatal que afecta a população caucasiana. Esta patologia é causada por mutações no gene que codifica a proteína responsável pela produção do suor, sucos digestivos e muco. Geralmente, mutações neste gene provocam um transporte anormal de iões através do epitélio das vias aéreas, causando a produção de muco excessivamente espesso e viscoso. Em vez de servir como lubrificante, o muco obstrui as vias aéreas, dificultando a ventilação e levando ao desenvolvimento de infecções crónicas. A natureza viscosa deste muco também afecta o sistema digestivo, uma vez que obstrui o pâncreas, impedindo que as enzimas cheguem aos intestinos. Estima-se que, a nível mundial, cerca de 70,000 crianças e jovens adultos sejam afectados pela fibrose cística, com 30,000 casos apenas nos Estados Unidos da América. A fibrose cística é tipicamente diagnosticada na infância e a actual esperança média de vida encontra-se, aproximadamente, nos 37 anos.

Actualmente, grande parte dos métodos para diagnóstico e monitorização de doenças pulmonares fornecem apenas uma medida global da função pulmonar, como ocorre no caso da espirometria. Por outro lado, a maioria das técnicas de imagiologia, usadas para avaliar as alterações morfológicas das vias aéreas e parênquima pulmonar, dão informação a nível regional, mas requerem o uso de radiação ionizante. Este factor é altamente indesejável, considerando a necessidade da realização frequente de exames na população pediátrica, que é mais sensível às propriedades carcinogénicas da radiação ionizante.

Hélio-3 e Xénon-129 hiperpolarizados têm sido usados como agentes de contraste em ressonância magnética durante mais de uma década, possibilitando a geração de imagens do sistema respiratório, através desta técnica. O facto de não envolverem radiação ionizante torna a utilização destes gases para monitorização de doenças pulmonares muito apelativa. Apesar do uso de Xénon-129 ter sido limitado pela reduzida intensidade de sinal que gerava em ressonância magnética em comparação com o Hélio-3, o seu custo reduzido devido à sua abundância natural e as recentes melhorias nas técnicas de polarização fazem com que este gás seja fortemente considerado para uso em imagiologia médica.

Todavia, a propriedade mais atraente do Xénon-129 é a sua solubilidade em tecidos que contenham água e lípidos, permitindo que se difunda facilmente através das membranas celulares. Uma vez inalado, a maior parte do Xénon-129 permanece sob forma de gás nos alvéolos, enquanto 1 a 2% dissolve-se no parênquima pulmonar e nos glóbulos

vermelhos do sangue. Dado que a frequência de ressonância do Xénon-129 é fortemente influenciada pelo meio, um desvio químico ocorre para este gás em diferentes compartimentos pulmonares: a frequência do Xénon-129 dissolvido no tecido e nos glóbulos vermelhos é desviada de cerca de 200 partes por milhão da frequência do Xénon-129 sob forma de gás, tornando possível diferenciar as fases gasosa e dissolvida, através de espectroscopia. Deste modo, a quantidade relativa de Xénon-129 em cada compartimento pode ser deduzida através da frequência e integral do sinal gerado.

A técnica descrita neste trabalho é denominada de 3D SB-CSI (imagiologia tridimensional por desvio químico numa inalação) e foi desenvolvida pelo grupo do Departamento de Radiologia e Imagiologia Médica da Universidade da Virgínia. A 3D SB-CSI combina o uso de Xénon-129 hiperpolarizado com espectroscopia por ressonância magnética para obter, numa só inalação, informação regional acerca da distribuição de gás nos alvéolos e da absorção e/ou troca do mesmo pelo tecido e glóbulos vermelhos. A implementação desta técnica tem como finalidade a detecção de alterações fisiológicas que possam ocorrer nível da ventilação, estrutura do tecido ou fluxo sanguíneo derivadas de uma condição patológica. Desta forma, é possível a obtenção de imagens de alta resolução que permitem a avaliação de uma das funções fisiológicas pulmonares mais básicas, de uma forma não-invasiva, não recorrendo ao uso de radiação ionizante.

Este estudo teve como objectivo demonstrar a eficácia da 3D SB-CSI para avaliar a distribuição de Xénon-129 nos diferentes compartimentos pulmonares em sujeitos com fibrose cística e em sujeitos saudáveis.

Nove estudos clínicos independentes foram realizados em sete voluntários: três saudáveis, três previamente diagnosticados com fibrose cística e um indivíduo fumador passivo, para investigar se a 3D SB-CSI é sensível a outros tipos de doenças respiratórias; um indivíduo saudável e um com fibrose cística foram examinados duas vezes para determinar a repetibilidade da técnica. Mapas de Xénon-129 hiperpolarizado como gás nos alvéolos e dissolvido no tecido e nos glóbulos vermelhos foram gerados para cada sujeito. Foi, igualmente, obtida a razão entre o gás dissolvido no tecido e nos glóbulos vermelhos, permitindo-nos inferir acerca da espessura da membrana pulmonar, que pode ser aumentada devido aos processos inflamatórios que ocorrem na fibrose cística.

Os resultados obtidos demonstraram uma distribuição de Xénon-129 nos alvéolos, tecido e glóbulos vermelhos uniforme, nos indivíduos saudáveis. A 3D SB-CSI também foi capaz de detectar um gradiente de intensidade crescente entre zonas mais anteriores e zonas mais posteriores dos pulmões, possivelmente atribuível ao efeito da gravidade mais

acentuado nas zonas dependentes. Estes gradientes fisiológicos são normais e já foram demonstrados em outros estudos em indivíduos saudáveis.

Por outro lado, vários defeitos, identificados pela redução ou inexistência de sinal, foram observados nos mapas de todos os compartimentos pulmonares nos sujeitos com fibrose cística, indicando que a actual resolução da imagem é suficiente para detectar alterações regionais. Foi, também, possível detectar a falta de gradiente causado pelo efeito da gravidade num sujeito em estágio mais avançado de fibrose cística.

A análise da alteração da espessura da membrana pulmonar com a doença demonstrou ser um método fiável para distinguir os sujeitos saudáveis e os com fibrose cística. Uma menor absorção e/ou troca de gás entre o tecido e os glóbulos vermelhos foi observada nos indivíduos com fibrose cística, provavelmente devido à inflamação da membrana pulmonar. Através o cálculo da razão entre a quantidade de gás dissolvido no tecido e nos glóbulos vermelhos, foi igualmente possível detectar doença no fumador passivo, não detectável na espirometria nem em imagens de ventilação convencionais utilizando Xénon-129. Estes resultados sugerem que a 3D SB-CSI poderá fornecer informação adicional útil para diagnosticar patologias que afectem a absorção e/ou troca de gases, como no caso em que ocorrem alterações ao nível da membrana pulmonar.

Esta técnica também demonstrou ser capaz de obter resultados reproduzíveis tanto para a população saudável como para a com fibrose cística. O indivíduo com patologia esteve associado a diferenças médias mais elevadas entre aquisições consecutivas, o que era esperado, dado que sujeitos com doenças pulmonares têm dificuldade em reproduzir os movimentos respiratórios.

Os resultados preliminares apresentados neste estudo permitem-nos supor que a 3D SB-CSI é capaz de fornecer informação detalhada ao nível da fisiologia pulmonar, em apenas uma inalação de gás e sem recurso a radiação ionizante. Uma vez que a maioria das técnicas de imagiologia usadas para monitorizar as doenças respiratórias não são recomendadas para a população pediátrica, devido às suas potenciais propriedades carcinogénicas, esta técnica pode tornar-se no método de escolha para avaliação de doenças pulmonares, em particular para o caso de fibrose cística.

Com o desenvolvimento de novas estratégias terapêuticas para o tratamento de fibrose cística, surge uma necessidade crescente de um melhor conhecimento da fisiologia pulmonar e mecanismos de progressão da doença. Para além disso, a avaliação da eficácia destas terapias tem sido restringida, devido às limitações dos actuais métodos de monitorização. Uma vez que a maior parte da investigação nesta área tem se focado em

estratégias anti-inflamatórias, a implementação da 3D SB-CSI poderá proporcionar um prognóstico mais precoce acerca do efeito do tratamento, já que demonstrou ser sensível a esta condição.

Palavras-chave: fibrose cística, Xénon-129 hiperpolarizado, espectroscopia por ressonância magnética, ventilação, absorção e/ou troca de gases.

Acknowledgments

Support comes in many forms. This space is dedicated to those who helped me, each one in their own way, throughout this journey.

To my advisor, Jaime Mata, for providing me the opportunity to learn and helping me grow as a researcher and a person.

To my second advisor, Eduardo Ducla-Soares, the greatest gratitude for five years of constant support. There is nobody I trust more to guide my academic path.

To my friends, old and new, Sara, Catarina, Joana, Sofia e Rafa, for bringing amusement into years of hard work and a piece of Portugal to the other side of the ocean.

To Márcia, my roomie for ten months, for walking, tripping and getting up with me for the last five years.

To my family, for the never-ending motivation. To my aunt and grandma, for making your place a second home for me.

At last, but certainly not least, to the most important people in my life: my dad who always pushed me to do better and my mom that always stood by my side, even when I was wrong. Thank you for believing in me.

Contents

Abstract.....	iv
Resumo	v
Acknowledgments	ix
List of Tables.....	xii
List of Figures.....	xiii
List of Acronyms	xvi
Introduction	1
Chapter I: Hyperpolarized Xenon-129 and chemical shift imaging to evaluate lung physiology	3
1.1 Magnetic resonance lung imaging: general considerations	3
1.2 Hyperpolarized Gas Imaging	4
1.2.1 MR signal generation: polarization	4
1.2.1.1 Optical pumping spin-exchange polarization process	5
1.2.2 Sequence considerations and MR hardware prerequisites	6
1.3 Hyperpolarized He-3 versus Hyperpolarized Xe-129	7
1.4 Xe-129 spectroscopy studies: measuring gas uptake-exchange in the lungs.....	8
1.4.1 3D Single Breath-hold Chemical Shift Imaging.....	11
Chapter II: Clinical application of 3D SB-CSI: cystic fibrosis	14
2.1 About Cystic fibrosis	14
2.2 Cystic fibrosis: diagnosis and monitoring	15
2.3 Materials and Methods.....	16
2.3.1 Subject characteristics	16
2.3.2 Polarization.....	17
2.3.3 MR scans	18
2.3.4 Spectroscopy data: signal processing	19

2.3.5	Spectroscopy data: map generation and quantification	22
2.3.5.1	Map generation	22
2.3.5.2	Map quantification.....	24
2.4	Results.....	25
2.4.1	Healthy versus Cystic fibrosis subjects	26
2.4.1.1	Map generation	26
2.4.1.2	Map quantification.....	28
2.4.2	Second-Hand Smoker subject.....	30
2.5	Discussion.....	32
	Conclusion.....	34
	References	36

List of Tables

Table 1 Current imaging modalities of interest in pulmonary drug research. Adapted from: [1].	4
Table 2 MR characteristics of HP He-3 and HP Xe-129 compared with H-1. Adapted from: [2, 3].	5
Table 3 Subject data.	17

List of Figures

Figure 1 Depiction of the alveolar-capillary unit (A) and corresponding Xe-129 spectroscopy signal in arbitrary units (AU) from the tissue (B) and RBC (C) for barrier thicknesses ranging from 1-7.5 μm and constant capillary diameter (8 μm). The detection of the RBC signal is delayed as barrier thickness increases. Adapted from: [11].....	9
Figure 2 Representative Xe-129 spectrum from a human lung, showing peaks at 0, 198 and 218 ppm, which correspond to xenon in the airspaces, dissolved in the lung parenchyma and the red-blood cells. Note that the relative sizes of the spectral peaks, in arbitrary units (AU), do not reflect the actual Xe-129 distribution, since only about 1 to 2% of all the gas is in the dissolved-phase at any given time. The RF pulse is applied at the dissolved-phase frequency, having a FA that is maximum at this frequency, while the gas-phase experiences a FA less than 1°. Adapted from: [16].	10
Figure 3 Pulse sequence diagram for the 3D SB-CSI technique. A SINC RF pulse is used to excite the Xe-129 spins, while a slice selection gradient is applied in the z-plane (G_z). In the x- and y- planes are applied the phase and frequency encoding gradients (G_x and G_y) and then the transverse magnetization is measured by receive coils. At the end of each readout, spoiler gradients are added in all planes to eliminate all unwanted transverse magnetization before the next RF pulse.	13
Figure 4 Average life expectancy (in years) in cystic fibrosis throughout the years. The development of new treatment options has resulted in improved survival of patients, being the current median age of survival in the late 30s. Adapted from: [25].	14
Figure 5 Axial computed tomographic image of the lungs of a 14-year-old girl with cystic fibrosis, demonstrating some of the morphological features of the disease (white arrows), such as bronchial wall thickening, bronchiectasis, peripheral mucus plugging and dorsal consolidations. Adapted from: [28].	15
Figure 6 Xemed polarizer used in the Xe-129 studies performed at the Department of Radiology and Medical Imaging of the University of Virginia.	18
Figure 7 Fourier transform of an exponentially decaying time-domain signal yields a spectrum, whose real and imaginary parts have the absorption and dispersion mode Lorentzian shapes, respectively. The arrows represent the width at half length. Adapted from: [32].	19

Figure 8 Depiction of the effect of a phase shift on the spectrum. The corresponding x- and y- components of the time-domain signal are shown, as well as the real and imaginary parts of the spectrum. Depending on the phase of the signal, the real and the imaginary parts may contain an absorption or dispersion mode lineshapes or a mixture of both. Adapted from: [33].....	20
Figure 9 Representation of the post-processing methods used in this study, applied in the real part of a selected spectrum of a voxel of one of the subjects' lungs. (A) Spectrum without any treatment, showing dephasation of both gas and dissolved-phase peaks. (B) Spectrum with frequency dependent phase correction, resulting in absorption mode with a Lorentzian lineshape peaks. (C) Spectrum with phase correction, one time zero filling and a 50 Hz Lorentzian filter. As the RF pulse was applied at the dissolved-phase frequency, the software program uses that frequency as reference, so the gas peak is at around 200 ppm not 0 ppm, as usually represented. The amplitude is represented in arbitrary units (AU).....	21
Figure 10 Absolute of the spectrum represented in Figure 9C, revealing the broadening of all peaks. The amplitude is represented in arbitrary units (AU).....	22
Figure 11 Coronal Xe-129 CSI maps of a healthy subject's lungs central slice. Xe-129 in alveoli (ventilation), dissolved in tissue and in RBC maps, generated through (A) area integration of the real part of post-processed signal, (B) area integration of the absolute signal and (C) PCA of the real part of the spectrum. The contrast and brightness were maintained within maps corresponding to the same lung compartment.	24
Figure 12 3D SB-CSI acquisition of the whole lung. Coronal CSI maps of Xe-129 as gas in alveoli (ventilation) and dissolved in tissue and in RBC in (A) a healthy subject (subject 1), and (B) a subject with moderate cystic fibrosis (subject 5). Ventilation images of Xe-129 using a gradient echo (GRE) pulse sequence (A: TR 6.8 ms, TE 1.6 ms and in-plane resolution 4.4x4.4 mm ² ; B: TR 6.0 ms, TE 0.6 ms and in-plane resolution 7.5x7.5 mm ²) were matched slice by slice to CSI maps. Note the signal originated from the heart in the most anterior slices in the dissolved-phase maps and its absence in the ventilation maps. (C) Coronal, axial and sagittal views of the SHS's lungs (subject 4; tissue maps) obtained in a single breath hold. Contrast and brightness were maintained within maps corresponding to the same lung compartment.	26
Figure 13 Coronal Xe-129 ventilation and dissolved-phase maps of a central lung slice of all cystic fibrosis subjects included in this study, with respective predicted FEV ₁ values	

(FEV ₁ pred.). The amount of defects in all lung compartments correlated well with the spirometry values.....	27
Figure 14 Coronal Xe-129 maps of all lung compartments in a plane that contained the heart (most anterior). The myocardium and blood inside the heart cavities were seen in the dissolved-phase maps, but not in the ventilation map. The white arrow, in the ventilation map, refers to the artifact caused by the vibration of the diaphragm due to the RF pulse. .	28
Figure 15 Coronal tissue/RBC ratio maps of a (A) healthy subject (subject 3) and (B) cystic fibrosis subject (subject 6) with respective median and standard deviation (STD) values. The CF subject presents a higher median and STD values for all slices in comparison with the healthy subject.	29
Figure 16 Quantification of the ratio of Xe-129 dissolved in tissue to that in RBC maps of all subjects, in arbitrary units (AU). Each point corresponds to a ratio value of one slice of each subject, whose pulmonary function is expressed by a spirometry measurement (percentage of predicted FEV ₁). Subjects with the lowest predicted FEV ₁ values presented higher tissue/RBC ratios.....	30
Figure 17 HP MR imaging lung measurements of the second-hand smoker subject (subject 4). (A) Ventilation maps obtained through a GRE sequence using Xe-129 as a contrast agent (TR 6.0 ms, TE 0.6 ms and in-plane resolution 7.5x7.5 mm ²). (B) He-3 apparent diffusion coefficient (ADC) maps (TR 9.7 ms, TE 6.3 ms, in-plane resolution 3x3 mm ² and b-values 0 and 1.6 s/cm ²). (C) Quantification of Xe-129 CSI maps that express the amount of gas dissolved in tissue to that in RBC, in arbitrary units (AU). CSI quantification shows an increase in the tissue/RBC ratio most prominent in anterior slices, consistent with disease observed in He-3 ADC maps (white arrows).....	31

List of Acronyms

3D	Three dimensional
3D SB-CSI	Three dimensional Single Breath-hold Chemical Shift Imaging
ADC	Apparent diffusion coefficient
AU	Arbitrary units
CF	Cystic fibrosis
CFTR	Cystic fibrosis transmembrane conductance regulator
cm ²	Square centimeter
CSI	Chemical Shift Imaging
CT	Computed Tomography
DL _{CO}	Diffusing capacity of the lung for carbon monoxide
FA	Flip-angle
FEV ₁	Forced expiratory volume in one second
FID	Free induction decay
FVC	Forced vital capacity
GRE	Gradient echo
H-1	Hydrogen
He-3	Helium-3
HP	Hyperpolarized
Hz	Hertz
J	Joule
L	Liter
mL	Milliliter
mm	Millimeter
mm ²	Square millimeter
MR	Magnetic Resonance
ms	Millisecond
N ₂	Nitrogen
P0 ₂	Partial pressure of oxygen
PCA	Principal Component Analysis
PET	Positron Emission Tomography
ppm	Parts per million

Rb	Rubidium
RBC	Red blood cell
RF	Radiofrequency
s	Second
SHS	Second-Hand Smoker
SINC	Cardinal sine
SNR	Signal-to-noise ratio
SPECT	Single Photon Emission Computed Tomography
STD	Standard deviation
T	Tesla
T ₁	Longitudinal relaxation time
T ₂ [*]	Transverse relaxation time that accounts for field inhomogeneities
TE	Echo time
TR	Time to repetition
XACT	Xenon Alveolar Capillary Transfer
Xe-129	Xenon-129
XTC	Xenon polarization transfer contrast
μm	Micrometer
μs	Microsecond

Introduction

Cystic fibrosis (CF) is the most frequent lethal genetic disorder in Caucasians that primarily affects the lungs and digestive system. This disorder is characterized by mutations in the CF gene that cause the production of abnormally thick and viscous mucus. The obstruction of the airways by this mucus predisposes the individuals to chronic lung infections, which lead to progressive loss of pulmonary function.

Current methods of pulmonary disease diagnosis and monitoring tend to focus primarily on the lung as a whole, and predominantly on ventilation parameters, which are easier to assess, as in the case of pulmonary function tests. Most of the imaging techniques used for probing the morphological changes of the airways and the lung parenchyma provide regional information, but require the use of ionizing radiation. This is a highly undesirable feature considering the need for repeated assessments for intervention or therapy.

The method demonstrated in this work was pioneered by the group at the Department of Radiology and Medical Imaging of the University of Virginia and is termed three dimensional Single Breath-hold Chemical Shift Imaging (3D SB-CSI). This method makes use of hyperpolarized Xenon-129 gas and magnetic resonance spectroscopic imaging, for non-invasively, obtaining regional characterization of basic pulmonary physiological processes within the lung, as ventilation and gas uptake-exchange in multiple lung compartments, without the use of radioactive substances or ionizing radiation.

The aim of this study is to demonstrate the feasibility of this technique for assessing ventilation and gas uptake-exchange in lung tissue and in red blood cells in subjects with cystic fibrosis and in healthy subjects.

In chapter I, a brief introduction about hyperpolarized gas imaging, with focus on Xenon-129 as a contrast agent, will be done to contextualize the reader about this recent imaging technique. More specifically, previous work relating spectroscopy and Xenon-129 will be described in order to point out the underlying fragilities and how they were overcome in the 3D SB-CSI technique.

In the second chapter, a potential clinical application of the 3D SB-CSI technique will be discussed for detecting regional disease on CF subjects. The use of this technique will also be demonstrated in a subject with high second-hand smoking exposure. The

Regional Quantification of Lung Function in Cystic Fibrosis using hyperpolarized Xenon-129 and Chemical Shift Imaging

methods used to analyze the spectroscopy data, successful in distinguishing healthy from diseased subjects will be outlined, as other attempts done during the course of this study. Finally, the obtained results will be presented and discussed, as well as, further improvements necessary for optimization of this technique.

Chapter I:

Hyperpolarized Xenon-129 and chemical shift imaging to evaluate lung physiology

1.1 Magnetic resonance lung imaging: general considerations

Clinical imaging of the lungs has been performed with chest radiography, Computed Tomography (CT), Single Photon Emission Computed Tomography (SPECT) or scintigraphy, involving the use of ionizing radiation, inhalation of radioactive gases and aerosols [1]. Whereas CT and radiography imaging are mostly restricted to morphologic studies, functional nuclear medicine studies are limited by spatial and temporal resolution (Table 1). More recently, functional pulmonary studies have been achieved with Positron Emission Tomography (PET), capable of providing regional high-sensitivity mapping of ventilation and perfusion. However, increased exposure to ionizing radiation is a major drawback, especially for longitudinal studies for intervention or therapy [1].

In the past, magnetic resonance (MR) imaging has not been the modality of choice to image the lung, due to the low density of hydrogen ($H-1$) nuclei in the lung tissue that results in a reduced low signal-to-noise ratio (SNR), and the numerous air-tissue interfaces that lead to susceptibility artifacts and hence poor image quality [2-4].

In 1994, Albert et al. demonstrated the feasibility of using hyperpolarized (HP) gas as contrast agent to increase the MR signal from proton imaging [5]. The physical characteristics of Helium-3 ($He-3$) and Xenon-129 ($Xe-129$) make their use appealing for hyperpolarized gas imaging. They are the only stable, non-toxic and non-radioactive isotopes, with a nuclear spin of $1/2$. Administered by inhalation, these MR contrast agents will fill the airspaces, allowing lung imaging [2-4].

Regional Quantification of Lung Function in Cystic Fibrosis using hyperpolarized Xenon-129 and Chemical Shift Imaging

Technique	Spatial Resolution and Time Scale		Application	Main Characteristics
	Small Rodents	Humans		
CT	50-100 micrometers; seconds to minutes	~600 micrometers; <1 minute	Anatomical, functional	Ionizing radiation; poor soft tissue contrast
Scintigraphy	No	~20 millimeters	Functional	Planar information
SPECT	≤1 millimeter; ~20 minutes	~10 millimeters; 10-30 minutes	Functional	Ionizing radiation; radioisotopes have longer half-lives than those used in PET; sensitivity 10 to 100 times smaller than PET
PET	1-2 millimeters; ~20 minutes	~4 millimeters; ~20 seconds	Metabolic, functional, molecular	Ionizing radiation; high sensitivity (picomolar concentrations); cyclotron needed
MR imaging	80-140 micrometers; seconds to hours	1.5 millimeters; seconds to minutes	Anatomical, functional, molecular	High spatial resolution and soft tissue contrast; low sensitivity

Table 1 Current imaging modalities of interest in pulmonary drug research. Adapted from: [1].

1.2 Hyperpolarized Gas Imaging

1.2.1 MR signal generation: polarization

To better understand the need for polarization of He-3 and Xe-129, it is necessary to discuss the generation of the MR signal. The MR signal intensity (I) is proportional to:

$$I \propto P \times \rho \times \mu \times \sin(\alpha) \times \gamma \times B_0 \quad (1)$$

where P corresponds to spin polarization, ρ is the spin density, μ the dipolar magnetic moment, α the flip-angle (FA), γ the gyromagnetic ratio and B_0 the main magnetic field.

The polarization of spin-1/2 nuclei expresses the fraction of spins that are in the parallel state relative to the ones that are in the anti-parallel state with respect to the external magnetic field, before the excitation by the radiofrequency (RF) pulse. The ratio of this asymmetry dictates the strength of the MR signal and can also be given by:

$$P \cong \frac{\mu B_0}{k_B T} \quad (2)$$

in which k_B represents the Boltzmann constant and T the absolute temperature. In proton MR imaging the polarization level is determined by the Boltzmann equilibrium with $P = 5 \times 10^{-6}$ reached at $\mu = 1.411 \times 10^{-26}$ Joules (J)/Tesla (T), $B_0 = 1.5$ T, $T = 310$ Kelvin. However, the high H-1 spin density in most biological tissues (composed by water)

Regional Quantification of Lung Function in Cystic Fibrosis using hyperpolarized Xenon-129 and Chemical Shift Imaging

compensates for the low amount of polarization exhibited by hydrogen nuclei, yielding images with high SNR (Table 2).

Isotope	H-1	He-3	Xe-129
Achievable polarization levels	5×10^{-6}	Up to ~ 60%	Up to ~ 60%
Spin density (10^{19} atoms/cubic centimeter)	6690 ^a	2.37 ^b	2.37 ^b
Magnetic moment (10^{-26} Joules/Tesla)	1.411	1.074	0.388
Gyromagnetic ratio (MegaHertz/Tesla)	42.6	32.4	11.8
Blood solubility (%)	100	1	17

^a In water

^b At 1-bar pressure and 310 Kelvin

Table 2 MR characteristics of HP He-3 and HP Xe-129 compared with H-1. Adapted from: [2, 3].

As discussed previously, in the case of lung imaging, the amount of lung tissue is reduced, so gaseous contrast agents are inhaled to improve the visualization of lung structures. However, even after the inhalation, the concentration of these gases is too small to generate a measurable signal. To overcome this problem, a large non-equilibrium polarization is achieved, in which the nuclear magnetic moments of the gas atoms are hyperpolarized above the Boltzmann equilibrium.

The optical pumping spin-exchange method, described in the next sub-section, is commonly used to polarize He-3 or Xe-129 gas and involves a transfer of angular momentum between an alkali-metal and the noble gases atoms. As a result, He-3 or Xe-129 spins oriented anti-parallel to an external magnetic field are “pumped” to parallel states. The optical pumping metastability-exchange is another method used for hyperpolarization but, since is limited to He-3, it will not be described here [2-4].

1.2.1.1 Optical pumping spin-exchange polarization process

In the optical pumping spin-exchange method, the polarization process occurs in two consecutive steps. The first involves the interaction of an alkali-metal vapor, usually rubidium (Rb), with a resonant laser light, which results in a change of its electronic spins from $-1/2$ to $+1/2$. Subsequently, the electronic polarization of Rb is transferred to the noble-gas nuclear spins through collisions between the atoms of both elements. The

polarization transfer rate depends on Rb and noble-gas densities, laser power and temperature inside the glass cell, which can be adjusted for an optimized process [2-4].

The glass cell that contains the gas mixture is kept under an external magnetic field, during the entire process. The presence of nitrogen (N₂) is also required during the polarization of the noble gases for quenching the fluorescence of the excited alkali vapor atoms. In the case of Xe-129 polarization, natural helium (Helium-4) is added to the gas mixture to act as a buffer gas, increasing the pressure inside the glass cell [6, 7].

At the end of the polarization process, the Rb vapor is condensed and the extraction of the hyperpolarized gases is done cryogenically. As HP Xe-129 has shorter relaxation times, because of the greater dimensions of the Xenon atom in comparison with the Helium atom, the Xe-129 gas is stored frozen, minimizing T₁ (longitudinal relaxation time) decay, and thus reducing loss of polarization. This gas is solidified cryogenically, being separated from the N₂ and Helium-4 gases (the solidification point of the noble gas is higher). When ready to be used, the Xe-129 ice is sublimated with hot water [6, 7].

1.2.2 Sequence considerations and MR hardware prerequisites

One important consideration to have in mind when imaging with HP gases is that there is no signal recovery, i.e., the non-equilibrium polarization is not renewable [2-4]. After excitation with the RF pulse, the spins return to the distribution predicted by Boltzmann statistics. The T₁ signal decay is dictated by RF saturation and the paramagnetic effects of residual oxygen in the lung. Consequently, the longitudinal signal (M_z) decreases as function of the number of RF pulses (n) and the local partial pressure of oxygen (PO_2).

$$M_z(n, \alpha) = M_0 \cos^n(\alpha) \exp\left(\frac{-1}{\varepsilon} \int_0^{nTR} \Gamma_{PO_2}(t) dt\right) \quad (3)$$

where M_0 is the initial magnetization, TR the time to repetition, ε the body temperature and Γ_{PO_2} the relaxation rate due to local PO₂. Note also the dependence of the signal decay rate with the FA. Spectroscopy and imaging pulse sequence with HP gases have to be designed in order to effectively use the available magnetization, being aware that after a 90° pulse there is no magnetization available. By Equation 3, we are able to conclude that the rapid pulse sequences with the adoption of low FA are necessary to

conserve the longitudinal magnetization. FA lower than 90° decrease the amount of magnetization tipped into the transverse plane, maximizing the magnetization used for signal generation.

On the other hand, the nuclear magnetic moments of He-3 and Xe-129 are lower than that of H-1 (Table 2), leading to different Larmor precession frequencies. Thus, there are some necessary alterations regarding the equipment that should be taken into account. For instance, a broadband RF system is needed for transmission, reception and amplification of the signals, as well as a purpose-built RF coil tunable to the appropriate frequency.

As regards to principal magnetic field strength, the initial magnetization depends linearly on the gyromagnetic ratio but not on B_0 , so the magnetization available is independent of the field strength of the scanner (Equation 3). To this date, most studies have been performed in 1.5 T scanners, as artifacts have been reported when using higher field strengths [3, 8].

1.3 Hyperpolarized He-3 versus Hyperpolarized Xe-129

The use of He-3 for human lung imaging has been facilitated by its large gyromagnetic ratio, and achievable polarizations of 40% or greater (Table 2), providing high signal strengths [2-4]. There are various results in both animals and humans that demonstrate the potential of this gas in lung imaging [2-4, 9, 10]. Nevertheless, one major disadvantage can be pointed out regarding the use of He-3 that opens new possibilities for Xe-129. Since He-3 is obtained from tritium decay mainly occurring in the production of nuclear weapons, the world's stock is limited. Recently, the demands of this gas for homeland security purposes have increased the prices as the worldwide supply is diminishing, preventing its widespread use in the clinical setting.

Although the use of Xe-129 has been restricted by its low gyromagnetic ratio, which results in lower SNR, the advances in the polarization level, nearing 50% at large output volumes [6, 7], have made it possible for Xe-129 to be eligible for lung imaging (Table 2). On the other hand, its unlimited supply, as constituent of earth's atmosphere,

and the relatively low-cost of enriched Xe-129 have made its use much more affordable than He-3 [2, 3].

However, the most appealing feature for using Xe-129 is the solubility in lipid and water-containing tissues (Table 2), which allows this gas to easily diffuse through cell membranes [11-16]. The majority of Xe-129, when inhaled, exists as gas in the alveoli (gas phase) while a small fraction (~1 to 2%) is dissolved in the lung parenchyma (tissue) or in the red blood cells (RBC) [4, 16]. As the resonance frequency of Xe-129 is strongly influenced by its medium, a chemical shift occurs for this gas in different lung compartments: the frequencies of Xe-129 dissolved into the lung parenchyma and the RBC are shifted by about 200 parts per million (ppm) from the frequency of Xe-129 as gas, becoming possible to differentiate the gas- and dissolved-phases using spectroscopy [4, 14, 16]. For these reasons, it is expected that techniques that use Xe-129 gas will provide valuable insights into pulmonary uptake-exchange processes, essential for the evaluation and staging of pulmonary disease progression.

1.4 Xe-129 spectroscopy studies: measuring gas uptake-exchange in the lungs

The uptake-exchange of alveolar gases consists of two consecutively ordered components. The first is associated with the diffusion of the gas through a semi-permeable membrane, which constitutes the air-blood barrier, and is determined by thickness and surface-area of the membrane and the second component is related to hemoglobin-binding gases such as oxygen and carbon dioxide, and depends on the reaction rate with the blood volume.

The total thickness of the air-blood barrier is only a fraction of 1 micrometer (μm). Considering an average diffusion constant in tissue on the order of 2×10^{-5} square centimeters (cm^2)/second (s), xenon would equilibrate with the lung parenchyma and the blood within tens of milliseconds (ms) [13]. Therefore, this diffusion time is expected to be highly sensitive to certain pathological conditions (Figure 1). Any increase in this time period could indicate thickening of the pulmonary membranes, as occurs in certain lung pathologies, such as cystic fibrosis.

Regional Quantification of Lung Function in Cystic Fibrosis using hyperpolarized Xenon-129 and Chemical Shift Imaging

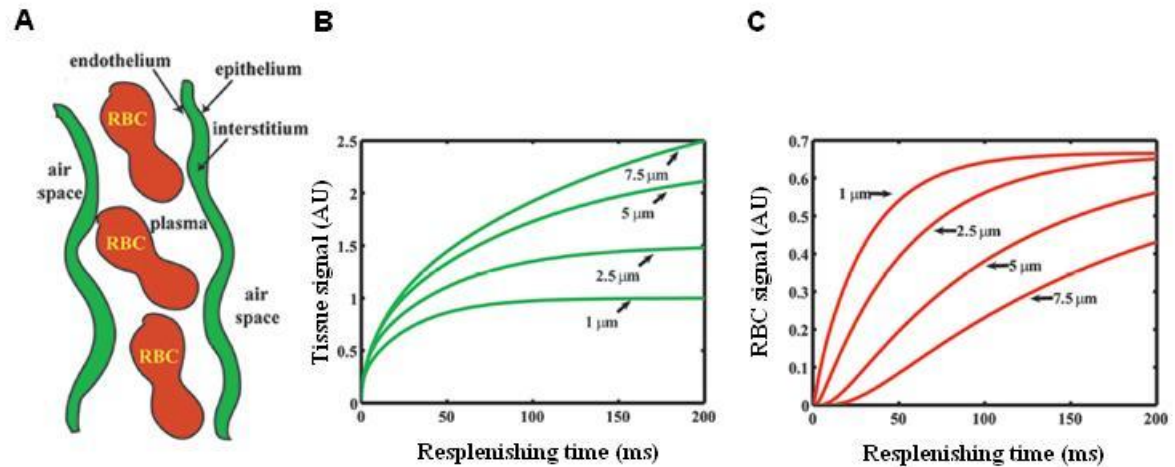


Figure 1 Depiction of the alveolar-capillary unit (A) and corresponding Xe-129 spectroscopy signal in arbitrary units (AU) from the tissue (B) and RBC (C) for barrier thicknesses ranging from 1-7.5 μm and constant capillary diameter (8 μm). The detection of the RBC signal is delayed as barrier thickness increases. Adapted from: [11].

The uptake of alveolar gases or diffusion capacity is commonly measured using carbon monoxide (DL_{CO}), which is the primary mean of directly assessing gas uptake and diagnosing pathologies that might affect the gas exchange. Unfortunately, DL_{CO} only provides a global measurement of gas uptake and cannot present heterogeneity caused by disease [12]. Alternatively, the diffusing capacity can be indirectly estimated by imaging techniques that provide regional information about this parameter. As mentioned before, HP Xe-129 has been presented as a great candidate for, non-invasively probing gas exchange-uptake through MR spectroscopy [11-16].

Depending on the resolution and the time available for the xenon to dissolve, spectroscopy using this gas generates a spectrum with three distinct peaks, each one associated with Xe-129 in a different physiological compartment. Gaseous Xe-129 in the major airways, bronchioles and alveolar spaces originates a peak at 0 ppm and is usually used as a reference. Two broad and partially overlapping peaks are also observed at around 198 ppm and 218 ppm, arising from Xe-129 dissolved in lung tissue and bound to hemoglobin inside the RBC, respectively (Figure 2) [12, 16].

High-quality images of the dissolved-phase are extremely difficult to obtain because only a small fraction of gas (~ 1 to 2%) gets dissolved in the lung parenchyma or in the RBC at a certain time [4, 16]. As a result, the gas signal has a large component in the MR spectrum, even with a narrow-band RF pulse centered at the frequency of the dissolved-phase peaks (Figure 2).

Regional Quantification of Lung Function in Cystic Fibrosis using hyperpolarized Xenon-129 and Chemical Shift Imaging

Regarding spectroscopy measurements done to characterize the Xe-129 gas uptake and exchange in the lungs, three techniques are worth to mention.

Swanson et al. in 1999 directly imaged Xe-129 in the dissolved phase of the rat's lung by using chemical shift imaging (CSI) [17]. However, the resulting maps were just a rough presentation of the animal's lungs due to the large voxel size (poor resolution) and low gas polarization (~5%). Also, this previous implementation of CSI required multiple breath-holds, mechanical ventilation and imaging for 8 minutes, which is not feasible for clinical applications.

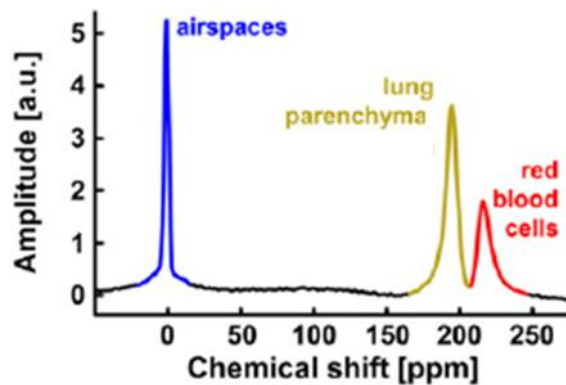


Figure 2 Representative Xe-129 spectrum from a human lung, showing peaks at 0, 198 and 218 ppm, which correspond to xenon in the airspaces, dissolved in the lung parenchyma and the red-blood cells. Note that the relative sizes of the spectral peaks, in arbitrary units (AU), do not reflect the actual Xe-129 distribution, since only about 1 to 2% of all the gas is in the dissolved-phase at any given time. The RF pulse is applied at the dissolved-phase frequency, having a FA that is maximum at this frequency, while the gas-phase experiences a FA less than 1°. Adapted from: [16].

An alternative imaging method retains higher spatial resolution while probing the gas exchange processes and is termed xenon polarization transfer contrast (XTC) [13-15]. This method is based on the attenuation of Xe-129 in the airspace after RF irradiation of the dissolved phase to map Xenon exchange between gas- and dissolved-phases. The magnetization of the dissolved-phase is saturated in the way that a permanent label is applied and the atoms cannot return to unlabeled state through relaxation. The only way to restore the unlabeled state is by the exchange through diffusion with the unlabeled atoms from the gas phase, decreasing the gas-phase magnetization. The main disadvantage of this technique is that it does not distinguish Xe-129 signals originating from different dissolved-phase compartments.

Another method was demonstrated by Driehuys et al. to overcome this problem, known as Xenon Alveolar Capillary Transfer (XACT) [11]. This method is based on the

Dixon imaging technique, developed to separate water from fat containing tissues in MR images. The XACT takes advantage of the difference in resonance frequency of the gas dissolved in the tissue and in RBC to image them at a specific phase shift. However, this technique cannot distinguish the signals from different lung compartments in a single breath inhalation.

The method demonstrated in this work and pioneered by the group at the Department of Radiology and Medical Imaging of the University of Virginia is the first capable of obtaining three dimensional (3D) characterization of gas distribution and uptake-exchange into the lung parenchyma and the red-blood cells, separately and in a single breath-hold. This technique combines the use of CSI and HP Xe-129, having sufficient resolution to detect defects in all lung compartments and is denominated 3D Single Breath-hold Chemical Shift Imaging [18-21].

1.4.1 3D Single Breath-hold Chemical Shift Imaging

The pulse sequence employed in the 3D SB-CSI technique was created by modification of a standard CSI pulse, allowing it to be used with HP Xe-129.

Atomic nuclei are surrounded by electrons that can shield the magnetic field, reducing the net magnetic field experienced by nuclear spins. Therefore, protons in different microscopic environments resonate at slightly different frequencies as a result of this shielding. The frequency separation (Δf_{cs}) between protons from different surroundings is obtained by:

$$\Delta f_{cs} = \frac{\gamma B_0}{2\pi} \Delta\delta \times 10^{-6} \quad (4)$$

where $\Delta\delta$ is the chemical shift in ppm.

A plot of the MR signal intensity of a certain object versus the chemical shift constitutes a spectrum. RF pulses that are designed to selectively excite or invert certain regions in the spectrum are denominated spectrally selective pulses. Every RF pulse has a corresponding frequency response, which can be calculated by solving the Bloch equations [22]. For example, a cardinal sine (SINC) function RF pulse yields a rectangular frequency

response. For a given pulse shape, the width of the frequency response (i.e. bandwidth in Hertz - Hz) is inversely proportional to the RF pulse width (in ms). Applied simultaneously with a gradient, the frequency response of an RF pulse is converted to a spatial profile, whereas without a gradient, the frequency response originates a single spectral profile. For spins whose resonance frequency is inside the profile, the pulse plays its designed functions. Outside the profile, the pulse has no effect on the spins.

The Single Breath-hold Chemical Shift Imaging (SB-CSI) technique exploits the fact that, once inhaled, HP Xe-129 dissolves in the lung parenchyma while diffusing and binding to hemoglobin, inside the RBC. Once dissolved, Xe-129 produces distinct MR signals (“peaks”) that are shifted in resonant frequency from the main gaseous Xe-129 peak. Thus, the relative amount of Xe-129 in each compartment (in RBC, tissue, or alveolar airspaces) can be deduced from the frequency and integral of its peak.

In order to create a CSI pulse sequence with high-resolution and an acquisition time in the same order as a breath-hold, the entire pulse sequence had to be redesigned.

Since there is no recovery of the longitudinal magnetization after excitation by the RF pulse, the TR of the pulse sequence could be reduced to a minimum, limited only by the HP Xe-129 diffusion rate between the alveoli, parenchyma and RBC. This allows the same number of voxels to be acquired in shorter acquisition times. A further compaction of the pulse sequence could also be achieved by reducing the time of the spoiling/dephasing gradients at the end of each TR (Figure 3). Concurrently, the amplitude of the same gradients is increased, resulting in an identical net area, so that the initial dephasing effect is retained.

To optimize the use of the available HP Xe-129 signal, other approaches were implemented.

Since the transverse relaxation time that accounts for field inhomogeneities (T_2^*) of dissolved HP Xe-129 is short, 1.5 to 2.4 ms at 1.5 T [12], echo time (TE) had to be reduced to less than 2.4 ms, thus minimizing signal loss due to decreasing levels of transverse magnetization.

A RF flip-angle of less than 30° per voxel was also chosen, instead of the traditional more than 30° used in this type of sequence [23]. A low FA permits maximizing the magnetization available for signal generation, since a smaller amount of longitudinal magnetization is tipped into the transverse plane. For each excitation, an RF pulse with

Regional Quantification of Lung Function in Cystic Fibrosis using hyperpolarized Xenon-129 and Chemical Shift Imaging

bandwidth 3125 Hz, which corresponds approximately to the frequency separation of gas and dissolved-phases, and duration 1280 microseconds (μs), was applied at the frequency of the Xe-129 in the dissolved-phase. This frequency is at, approximately, 200 ppm from that of HP Xe-129 gas in the airspaces [4, 14, 16].

The modifications described above permit scan times of less than 15 s, which is an important feature for imaging patients with pulmonary disease that cannot hold their breath for larger periods.

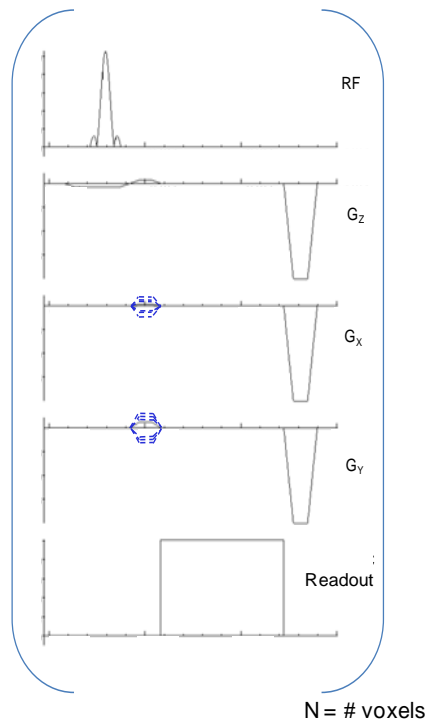


Figure 3 Pulse sequence diagram for the 3D SB-CSI technique. A SINC RF pulse is used to excite the Xe-129 spins, while a slice selection gradient is applied in the z-plane (G_z). In the x- and y- planes are applied the phase and frequency encoding gradients (G_x and G_y) and then the transverse magnetization is measured by receive coils. At the end of each readout, spoiler gradients are added in all planes to eliminate all unwanted transverse magnetization before the next RF pulse.

Chapter II:

Clinical application of 3D SB-CSI: cystic fibrosis

2.1 About Cystic fibrosis

Cystic fibrosis (CF) is the most common, fatal, inherited disease in the Caucasian population. CF is caused by a mutation in the gene responsible for production of the protein cystic fibrosis transmembrane conductance regulator (CFTR), required to regulate the components of sweat, digestive juices, and mucus. Usually, mutations in the CFTR gene lead to abnormal transport of chloride ions across the airway epithelium, causing the production of unusually thick and viscous mucus. Instead of serving as a lubricant, the mucus clogs the airways, impairing lung ventilation and creating an ideal breeding ground for chronic airway infections. Permanent lung damage might include formation of scar tissue (fibrosis) and cysts. The thick mucus also obstructs the pancreas, preventing enzymes from reaching the intestines to digest food [24, 25].

It is estimated that about 70,000 children and young adults have been diagnosed with CF worldwide, with 30,000 cases only in the United States. This disorder is typically diagnosed in early infancy by a sweat test or before birth by genetic testing [25].

Due to the advances in clinical care and medical research of the past decades, the life expectancy of CF patients has increased substantially (Figure 4), being the current median age of survival in the late 30s [24, 25]. Although cystic fibrosis is not yet curable, clinical studies to test the potential of a variety of treatments have been

Average Life Expectancy in Cystic Fibrosis

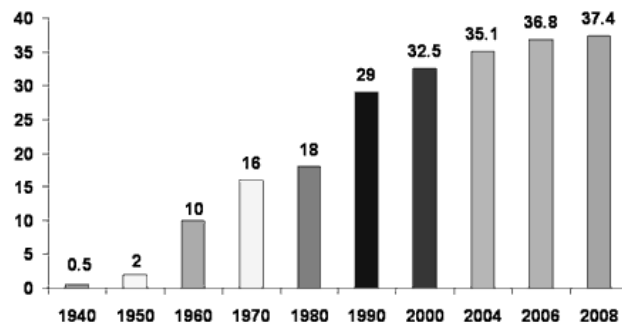


Figure 4 Average life expectancy (in years) in cystic fibrosis throughout the years. The development of new treatment options has resulted in improved survival of patients, being the current median age of survival in the late 30s. Adapted from: [25].

performed, many of them focused on therapeutic anti-inflammatory strategies [25, 26]. Clinical trials of a new drug therapy approved by the Food and Drug Administration in January 2012, Kalydeco™, (Ivacaftor, Vertex, United States), which is classified as a CFTR potentiator, showed promising preliminary results. This new drug is indicated for the treatment of CF in patients 6 years of age and older who have a specific mutation in the CFTR gene [25, 27]. In extreme situations, lung transplantation may be considered when lung function is reduced to the point where assistance from mechanical devices is required for patient survival [25].

2.2 Cystic fibrosis: diagnosis and monitoring

Monitoring of disease progression and efficacy of treatments plays an important role in improving the prognosis in CF. A decrease in the pulmonary function test parameter forced expiratory volume in one second (FEV₁) was shown to be the best prognostic factor for the course of the disease and the most significant predictor of mortality in a study done

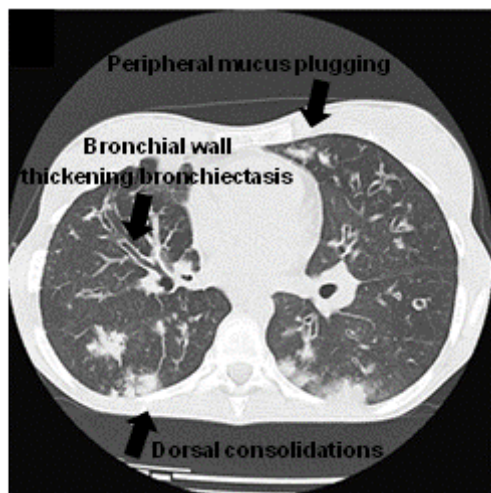


Figure 5 Axial computed tomographic image of the lungs of a 14-year-old girl with cystic fibrosis, demonstrating some of the morphological features of the disease (white arrows), such as bronchial wall thickening, bronchiectasis, peripheral mucus plugging and dorsal consolidations. Adapted from: [28].

with CF patients [28, 29]. However, pulmonary function tests give no regional information about lung morphology or function, providing only a global assessment of ventilation parameters, which can mask focal disease and regional changes with treatment. Moreover, this method is highly dependable on patient effort and collaboration, being difficult to perform in young children [26, 28].

The morphological features of CF have been described in several studies [24, 28, 30]. Extensive inflammation of the bronchial walls was found in CF lungs when compared to controls [24, 28, 30]. Other structural changes of

CF disease include bronchiectasis (destruction and widening of the airways), mucus plugging, consolidation and segmental-lobar destruction (Figure 5) [24, 28].

Of the imaging techniques used for probing the morphological changes of the airways and the lung parenchyma, chest x-ray is the most widely used modality. However, x-ray is not ideal for early assessments of the disease since it has limited sensitivity. CT has emerged as “the gold standard” to monitor the morphological changes related with CF and so far, it is the only reliable imaging method capable of monitoring early stages of CF lung disease [24].

Although CT is able to provide high temporal and spatial resolutions of the lung parenchyma, it exposes the patient to relatively high doses of ionizing radiation. This is an extremely undesirable feature considering the need for repeated assessments in pediatric patients, who are more sensitive to the carcinogenic properties of ionizing radiation. On the other hand, HP Xe-129 MR imaging allows high-resolution imaging, providing a way to evaluate regional lung function, without the risks associated with repeated exposure to ionizing radiation.

A better understanding of pulmonary disease progression, including the associated genetic and molecular pathways, is desirable. Currently, no imaging technique, suitable for clinical application, is able to provide a measurement of one of the most basic physiological lung functions that is the gas uptake-exchange in lung tissue and blood [16]. The implementation of the 3D SB-CSI technique aims to distinguish the physiological alterations that may occur at the ventilation, tissue structure or blood flow levels. This knowledge may allow for an earlier forecast of treatment responses and outcomes, as well as for the identification and correlation of physiologic alterations based on different genetic types of CF.

2.3 Materials and Methods

2.3.1 Subject characteristics

Nine independent clinical studies were performed in seven volunteers enrolled in this study (Table 3): 3 healthy (mean age: 19 years-old), 3 CF-previously diagnosed (mean age: 27 years-old) and 1 subject with high second-hand smoking exposure; one healthy and one CF were imaged twice for a repeatability study. All subjects were submitted to a baseline spirometry examination, including measurement of FEV₁ and forced vital capacity

Regional Quantification of Lung Function in Cystic Fibrosis using hyperpolarized Xenon-129 and Chemical Shift Imaging

(FVC), prior to the MR scan to determine eligibility and disease category. Subjects with $FEV_1 > 50\%$ and $FEV_1 < 70\%$ were considered in the moderate-CF category, and subjects with $FEV_1 \geq 70\%$ in the mild category. Healthy subjects had normal spirometry values ($FEV_1 \geq 80\%$ and $FEV_1/FVC \geq 0.70$) and no history of pulmonary disease.

All studies were supervised by a physician and the subject's heart rate and oxygen saturation levels were monitored throughout the MR session. All subjects were able to inhale HP Xe-129 and hold their breath for the scan duration. No relevant side effects were experienced by any of the volunteers, besides instant euphoria and a decrease in blood PO_2 .

Study no.	Subject no.	Age (years)	Sex	FEV_1 , % predicted	FEV_1/FVC	Health status
1	1	19	F	104	0.84	Healthy
2	2	21	F	112	0.88	Healthy
3	3	18	M	88	0.80	Healthy
4	3	18	M	88	0.80	Healthy
5	4	64	M	94	0.76	Second-Hand Smoker
6	5	19	F	55	0.54	Cystic Fibrosis (moderate)
7	6	24	F	71	0.70	Cystic Fibrosis (mild)
8	6	24	F	71	0.70	Cystic Fibrosis (mild)
9	7	37	M	87	0.66	Cystic Fibrosis (mild)

Table 3 Subject data.

2.3.2 Polarization

Isotopically enriched (~87%) Xe-129 was polarized via optical-pumping spin-exchange to approximately 35 to 50% using a commercial prototype system (Xemed LLC, United States).

To overcome the low gyromagnetic ratio of Xe-129 (of almost three times lower than the gyromagnetic ratio of He-3) and provide an elevated image SNR, high polarization levels must be achieved.

The Xemed polarizer (Figure 6) used in this study is the only one capable of reaching polarization levels of 50% with high output volumes, as a result of some design modifications [6, 7].

A spiral trajectory is used for the glass cell, in order to increase the volume of Rb vapor polarized by the laser. This strategy is also employed when the Xe-129 ice is sublimated, achieving a more efficient process by increasing the surface-to-volume ratio of

Regional Quantification of Lung Function in Cystic Fibrosis using hyperpolarized Xenon-129 and Chemical Shift Imaging

the ice in contact with hot water. Moreover, oil is used to heat the glass cell, instead of high pressure air, permitting less variation of temperature. With these improvements and the application of 1200 Watts of laser power, the Xemed polarizer is able to polarize 2 Liters (L) of Xe-129 with high polarization levels (35 to 50%) in 15 minutes. Prior to the MR scans, HP Xe-129 was dispensed into Tedlar bags and transported to the MR scanner across the hallway.



Figure 6 Xemed polarizer used in the Xe-129 studies performed at the Department of Radiology and Medical Imaging of the University of Virginia.

2.3.3 MR scans

All scans were done in a 1.5 T clinical system (Avanto, Siemens Medical Solutions, United States) using a linear transmit/receive RF coil built in-house and tuned to the Xe-129 frequency. The subjects were positioned supine on the MR table with the chest coil strapped around their chest and placed into the scanner at the isocenter. A set of 3D proton scout localizer MR images were obtained to confirm the position of the lungs at the isocenter and to determine positioning of the Xe-129 acquisitions. The volume of gas administered to the subjects depended on their FVC values; for each acquisition, 700 to 900 milliliters (mL) of HP Xe-129 gas, mixed with room air or oxygen (230 to 500mL),

was inhaled by the subjects, followed by a breath-hold during the entire pulse-sequence acquisition. A matrix of 18x18x8 voxels, interpolated to 32x32x8 voxels, was positioned over the lungs, with a field-of-view of 320x320 to 350x350 square millimeters (mm²), corresponding to an in-plane resolution of 17.8x17.8 to 19.4x19.4 mm². The slice thickness varied from 25 to 31.25 millimeters (mm), TR was 27 ms and TE was 2.3 ms.

2.3.4 Spectroscopy data: signal processing

Xe-129 CSI post-processing was performed using the 3DiCSI (Qi Zhao, Columbia University, United States) software package.

In MR spectroscopy, the resulting data from the MR measurements, also known as free-induction decay (FID) response signal, is presented in the time-domain. In order to obtain the conventional spectrum, i.e., a frequency-domain signal, the data has to be Fourier Transformed. If the FID is obtained in a complex form, as occurs in this case, the Fourier transformation will give a complex frequency-domain signal, that is, composed by real and imaginary parts. The real part of the spectrum contains a peak with the absorption mode with a Lorentzian lineshape, whereas the imaginary part represents the dispersion mode, also with Lorentzian lineshape (Figure 7). The FID has also an arbitrary phase associated with it and the relative contributions of absorption and dispersion lineshape depend on the phase, i.e., the real part of the spectrum, and likewise for the imaginary part, may contain a mixture of absorption and dispersion modes (Figure 8) [31-33].

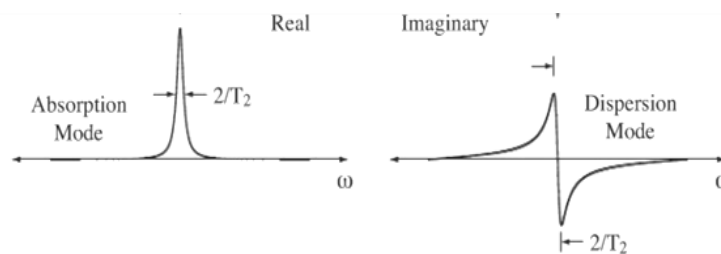


Figure 7 Fourier transform of an exponentially decaying time-domain signal yields a spectrum, whose real and imaginary parts have the absorption and dispersion mode Lorentzian shapes, respectively. The arrows represent the width at half length. Adapted from: [32].

In this case, it is necessary to make sure that the real part of the spectrum has the absorption mode lineshape as this corresponds to the narrowest peaks. Thus, to obtain a pure absorption mode, the phase must be corrected.

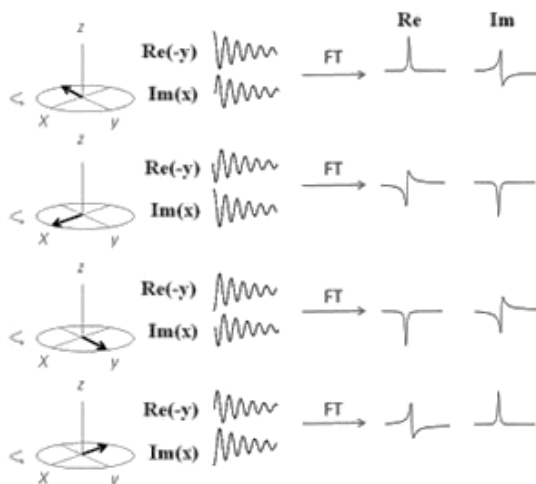


Figure 8 Depiction of the effect of a phase shift on the spectrum. The corresponding x- and y- components of the time-domain signal are shown, as well as the real and imaginary parts of the spectrum. Depending on the phase of the signal, the real and the imaginary parts may contain an absorption or dispersion mode lineshapes or a mixture of both. Adapted from: [33].

A constant phase correction is applied to the whole spectrum. However, in some cases the phase is not the same for all the peaks in the spectrum, varying from one edge to the other. One of the reasons for this to happen is attributable to the design of the RF pulse. This off-resonance effect can be corrected by introducing a factor that multiplied by the spectrum gives a phase correction proportional to the offset [31-33].

As mentioned before, the key aspect of the 3D SB-CSI technique is that it is able to separate the dissolved-phase peaks. For that, it may be necessary to obtain a better defined spectrum and one way to do it is through a post-processing method termed zero filling. The original FID is added an equal amount of zeros, so that the spectrum will have the double of its original length.

On the other hand, adding more points to the spectrum might result in increased noise, and consequently reduced SNR. Noise is classically described as ‘Gaussian with zero mean’, which means that the time average of the noise is zero and the probability of a certain amplitude to occur is proportional to a Gaussian function of the amplitude, that is, high amplitude spikes are less probable to occur than small amplitude spikes. The Fourier Transform does not alter the features of the noise: it retains both the Gaussian distribution

and the zero mean. It is also important to consider that a typical time domain signal has higher amplitude at the beginning, decaying over time, while the noise remains constant throughout. This suggests that the early fraction of the time-domain signal contains the most significant information of the signal. Thus, the later parts of the signal can be attenuated by multiplying the time-domain signal by a decaying weighting function. A common choice for a decaying function is a Lorentzian (only the right-hand half of the curve, i.e., time > 0). The decay rate of the filter must be chosen considering that the noise will not be attenuated significantly with slow rates, and fast rates may result in a reduction of peak height, thus leading to degradation of the SNR.

In Figure 9, the effects of the post-processing methods mentioned above are depicted in a spectrum corresponding to a pixel from a subject imaged through the 3D SB-CSI technique.

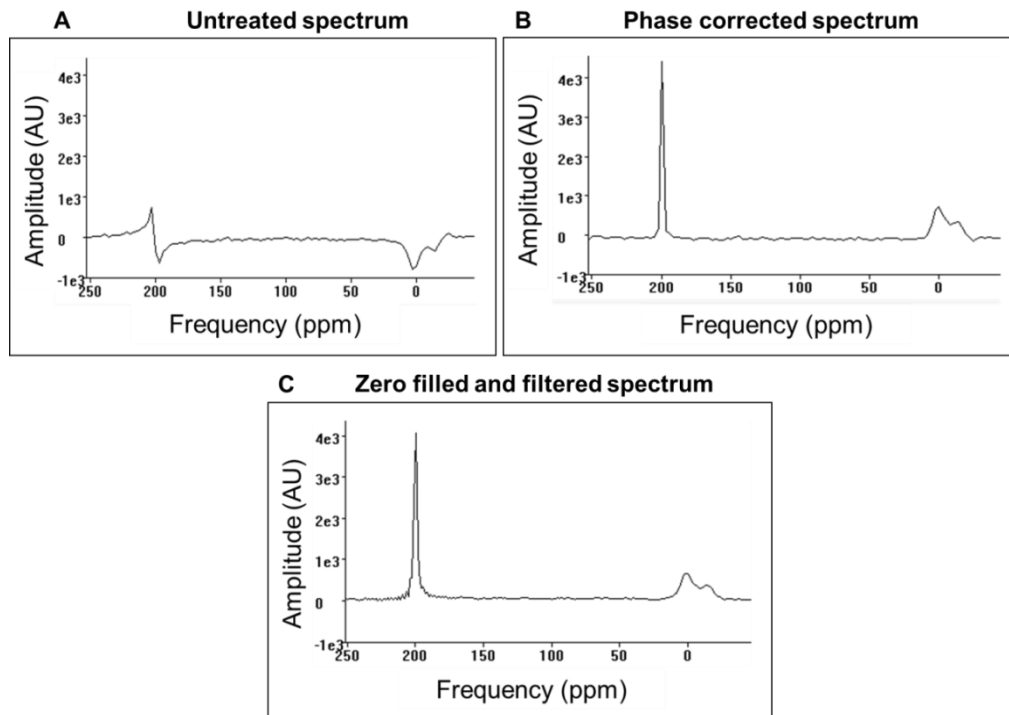


Figure 9 Representation of the post-processing methods used in this study, applied in the real part of a selected spectrum of a voxel of one of the subjects' lungs. (A) Spectrum without any treatment, showing dephasing of both gas and dissolved-phase peaks. (B) Spectrum with frequency dependent phase correction, resulting in absorption mode with a Lorentzian lineshape peaks. (C) Spectrum with phase correction, one time zero filling and a 50 Hz Lorentzian filter. As the RF pulse was applied at the dissolved-phase frequency, the software program uses that frequency as reference, so the gas peak is at around 200 ppm not 0 ppm, as usually represented. The amplitude is represented in arbitrary units (AU).

As mentioned before, some spectra exhibit a frequency dependent offset and thus a frequency dependent phase correction is required to obtain an absorption mode with a Lorentzian lineshape for all the peaks (Figure 9B). By comparing the phase corrected spectrum (Figure 9B) with the one combining zero filling and filtering with a 50 Hz Lorentzian decaying function (Figure 9C), we are able to notice that the latter is better defined, which is a desirable feature for determining peak intervals correctly. The decay rate was chosen in a way that the amplitude of the peaks was not significantly reduced, while maximizing noise attenuation.

Having in mind the considerations stated above, the time-domain data (FID) of each pixel from each slice was zero filled to 1024 points, filtered with a 50 Hz Lorentzian decaying function, Fourier Transformed and the real part corrected for phase shifts. Furthermore, the phase offset was not constant throughout the lungs, thus a phase correction had to be done manually for each outlier voxel of the lung. This heterogeneous dephasing effect might be related to multiple effects like: magnetic field inhomogeneities, movement of the heart and vibration of the diaphragm in the thoracic cavity or the RF pulse design. These effects will be addressed in the conclusion section.

2.3.5 Spectroscopy data: map generation and quantification

2.3.5.1 Map generation

In the majority of spectroscopy studies, the real part of the signal is used for quantifying the data, mostly because it corresponds to the narrowest peaks [31]. However, in circumstances where the phase correction is challenging, as in this case in which the phase shift is not uniform throughout the lung, the absolute signal can be used. The absolute signal has a contribution of both real and imaginary parts

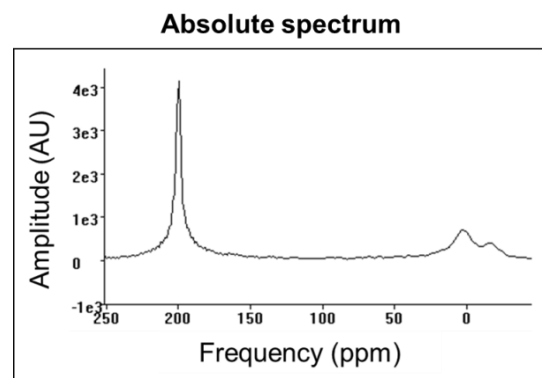


Figure 10 Absolute of the spectrum represented in Figure 9C, revealing the broadening of all peaks. The amplitude is represented in arbitrary units (AU).

and is phase independent, which results in broader peaks, as shown in Figure 10.

All maps depicted in Figures 11A and B were generated through area integration, i.e, the area under the curve is calculated considering a given interval. Corresponding ventilation, tissue and RBC maps created using the absolute signal (Figure 11B) are smoother and have better quality than the ones generated with the real part (Figure 11A).

It is also possible to note that the dissolved phase maps (tissue and RBC) appear identical, perhaps due to signal contamination from their very close spectral proximity at this magnetic field strength. Thus, Principal Component Analysis (PCA) was also applied to the real part of the signal in an attempt to obtain more distinction between the signals from the tissue and the RBC (Figure 11C). The aim of PCA is to reduce the quantity of spectral data, and thereby avoid overfitting, without discarding any useful information. PCA uses projections to extract from a greater number of variables, a much smaller number of new variables. Each of the new variables (principal components) is a linear combination of the original measurements and therefore contains information from the entire selected spectrum. In this case, the amplitude of the principal component with higher eigenvalue value (fraction of total variation of the data set that the principal component explains) is measured and displayed on a map [34]. However, the use of PCA did not appear to make a significant difference in separating the signals from the dissolved phase or increasing image quality. For this reason, area integration of the absolute signal was chosen for map generation.

In sum, ventilation, tissue and RBC maps were obtained calculating the area under the absolute peaks with the software package referenced in the previous section. Frequency shifts were observed in some subjects. However, the interval size of area integration of each peak was chosen to be constant among every slice of each subject and between subjects. Care was taken to cover as much of the peak data points as possible, while minimizing noise inclusion. In some cases, position of the inflexion point between the dissolved-phase peaks also changed in frequency throughout the lung. In these cases, a recurrent position was chosen.

The chemical shift of the dissolved-phase peaks in all subjects remained relatively invariable, being of 198 ± 1.0 ppm and 214 ± 1.4 ppm, for the tissue and RBC peaks, respectively. These values are in close agreement with the ones presented in section 1.2.4

Regional Quantification of Lung Function in Cystic Fibrosis using hyperpolarized Xenon-129 and Chemical Shift Imaging

and in [12, 16]. To improve image quality, the data was interpolated from a matrix of 32x32 to 128x128 voxels.

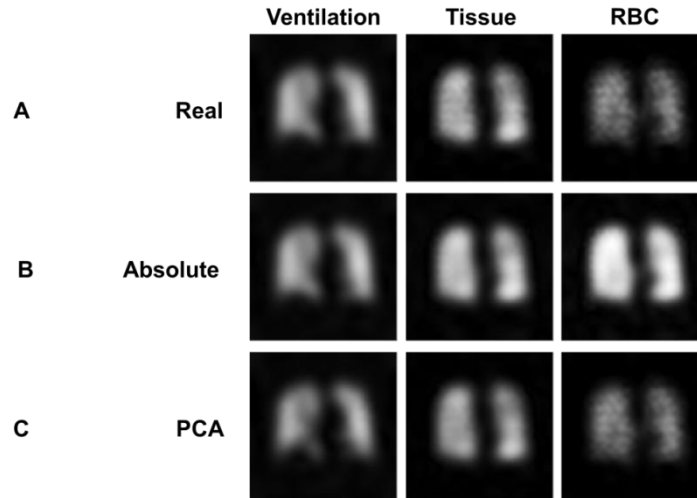


Figure 11 Coronal Xe-129 CSI maps of a healthy subject's lungs central slice. Xe-129 in alveoli (ventilation), dissolved in tissue and in RBC maps, generated through (A) area integration of the real part of post-processed signal, (B) area integration of the absolute signal and (C) PCA of the real part of the spectrum. The contrast and brightness were maintained within maps corresponding to the same lung compartment.

2.3.5.2 Map quantification

One of aims of this study was to find a quantification method capable of differentiating healthy from CF subjects. Area integration of a single peak does not provide meaningful information about physiological function that can be compared among subjects, regardless of the amount of gas inhaled and polarization level. The ratio of Xe-129 in the dissolved-phase to that in the gas-phase is commonly chosen as a normalization method [16]. However, with the data collected for this study, the normalized tissue and RBC ratios did not appear to be directly correlated with disease. The use of slightly different FA profiles might be a reasonable explanation for the variability in the amplitude of the dissolved-phase peaks relative to the gas peak among subjects of the same health status. Gas uptake and exchange in lung tissue and RBC can also be assessed by obtaining the ratio of gas dissolved in the tissue to that dissolved in the RBC. This will allow inferring about pulmonary membrane thickness, which can be increased in case of CF disease.

On the other hand, using the absolute part of the signal has also proven to be inefficient in distinguishing healthy from CF subjects. RBC peak broadening, observed in the absolute spectrum (Figure 10) and demonstrated by the higher intensities in the absolute RBC map (Figure 11B) compared to the corresponding map generated with the real part (Figure 11A), might be one of the reasons for this lack of distinction between subjects. As expected, as the RBC peak broadens, the quantification becomes less sensitive to minor deviations. Consequently, the data was quantified using the real part of the signal.

In short, 32x32 voxels maps of the ratio of Xe-129 dissolved in tissue to Xe-129 dissolved in RBC (tissue/RBC) were generated for the masked lung regions (to avoid the inclusion of noise), through area integration of the real part of the spectrum. This was performed for each slice of each subject using the same software package. Only coronal slices were quantified, since they are the most commonly chosen to evaluate respiratory physiology. The mean, median and standard deviation of each slice were calculated.

2.4 Results

With the 3D SB-CSI technique, three dimensional regional information of ventilation and gas uptake-exchange into different lung compartments was obtained, through acquisition of multiple-slices and multiple-planes, in order to cover the whole lung. Examples of the acquisition of multiple-slices are given in Figures 12A and B for a healthy (subject 1) and a moderate-CF subjects (subject 5), respectively, while multiple-planes of the Second-Hand Smoker (SHS) subject's lungs (subject 4) are depicted in Figure 12C.

In the next sections, the results of CSI map generation and quantification will be presented for healthy and CF subjects. The case of the SHS will also be analyzed in section 2.4.2.

Regional Quantification of Lung Function in Cystic Fibrosis using hyperpolarized Xenon-129 and Chemical Shift Imaging

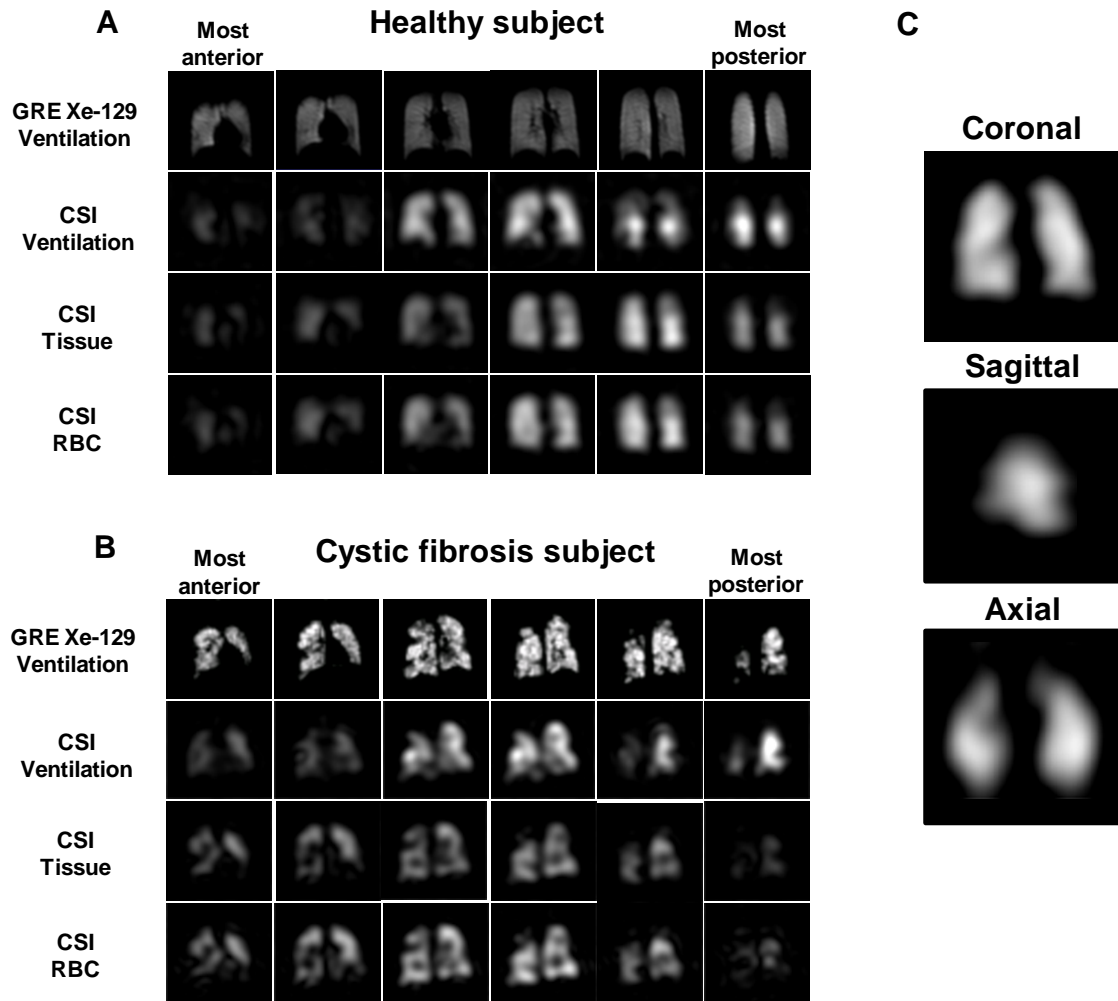


Figure 12 3D SB-CSI acquisition of the whole lung. Coronal CSI maps of Xe-129 as gas in alveoli (ventilation) and dissolved in tissue and in RBC in (A) a healthy subject (subject 1), and (B) a subject with moderate cystic fibrosis (subject 5). Ventilation images of Xe-129 using a gradient echo (GRE) pulse sequence (A: TR 6.8 ms, TE 1.6 ms and in-plane resolution 4.4x4.4 mm²; B: TR 6.0 ms, TE 0.6 ms and in-plane resolution 7.5x7.5 mm²) were matched slice by slice to CSI maps. Note the signal originated from the heart in the most anterior slices in the dissolved-phase maps and its absence in the ventilation maps. (C) Coronal, axial and sagittal views of the SHS's lungs (subject 4; tissue maps) obtained in a single breath hold. Contrast and brightness were maintained within maps corresponding to the same lung compartment.

2.4.1 Healthy versus Cystic fibrosis subjects

2.4.1.1 Map generation

Xe-129 maps of the gas in the alveoli (ventilation) as well as dissolved in the lung tissue and in RBC demonstrated that healthy subjects presented homogenous ventilation and gas uptake-exchange within the lung. (Figure 12A).

Regional Quantification of Lung Function in Cystic Fibrosis using hyperpolarized Xenon-129 and Chemical Shift Imaging

On the other hand, multiple regional defects (small areas with less or no detectable signal) could be observed in the CF subjects (Figures 12B and 13) in all three lung compartments, showing impaired ventilation, and consequently heterogeneous gas uptake by lung tissue and blood.

Increased ventilation, tissue density and perfusion were most visible in central-posterior slices of healthy subjects, as indicated by the higher signal intensities (Figure 12A).

Contrarily, tissue and RBC maps of the moderate-CF subject did not exhibit the same trend, as signal intensity did not seem to change significantly towards the posterior regions of the lung (Figure 12B).

Both healthy and CF subjects CSI ventilation maps presented in Figures 12A and B correlated well with direct MR ventilation images using traditional HP Xe-129 MR imaging techniques (GRE Xe-129 Ventilation).

The effect of different degrees of disease severity was also assessed by comparing the amount of defects in the maps of each lung compartment. As demonstrated in Figure 13, the moderate-CF subject (subject 5) showed whole lung heterogeneity, while the mild-CF subjects (subjects 6 and 7) only presented impaired ventilation and gas uptake-exchange in the superior portion of the lung. The very-mild CF subject (subject 7) had the fewest defects in the lungs, which correlated well with the predicted FEV₁ that is situated in the normal range.

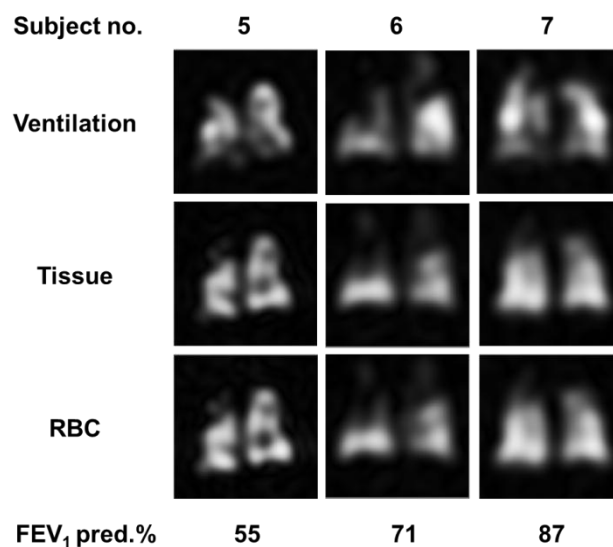


Figure 13 Coronal Xe-129 ventilation and dissolved-phase maps of a central lung slice of all cystic fibrosis subjects included in this study, with respective predicted FEV₁ values (FEV₁ pred.). The amount of defects in all lung compartments correlated well with the spirometry values.

Regional Quantification of Lung Function in Cystic Fibrosis using hyperpolarized Xenon-129 and Chemical Shift Imaging

The CSI maps presented here also showed that the tissue and RBC maps may provide additional information regarding lung physiology that cannot be deduced from the ventilation maps. Not only the dissolved-phase maps showed areas of the lungs with signal that may not be ventilated, signal from dissolved Xe-129 also appeared beyond lung tissue, for instance in the myocardium and blood inside the heart cavities. In Figures 12A and 14, those structures were seen in tissue and RBC maps and not in the ventilation map.

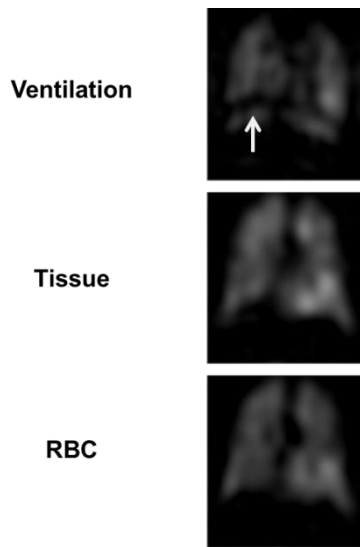


Figure 14 Coronal Xe-129 maps of all lung compartments in a plane that contained the heart (most anterior). The myocardium and blood inside the heart cavities were seen in the dissolved-phase maps, but not in the ventilation map. The white arrow, in the ventilation map, refers to the artifact caused by the vibration of the diaphragm due to the RF pulse.

2.4.1.2 Map quantification

The regional information presented on the tissue/RBC ratio maps shows a relatively homogenous distribution of the Xe-129 dissolved in tissue to Xe-129 dissolved in RBC in the healthy subjects (Figure 15A).

Conversely, in the CF subjects' maps, it was possible to observe focal elevations of this ratio, accompanied by a higher standard deviation value (STD) (Figure 15B). Most importantly, a median increase in the tissue/RBC ratio was detected in all slices, also noticeable by the existence of warmer colors in the maps. The median of the signal-containing voxels of the lungs was the statistical measure chosen to represent the data in order to minimize the influence of outliers in the distribution.

Regional Quantification of Lung Function in Cystic Fibrosis using hyperpolarized Xenon-129 and Chemical Shift Imaging

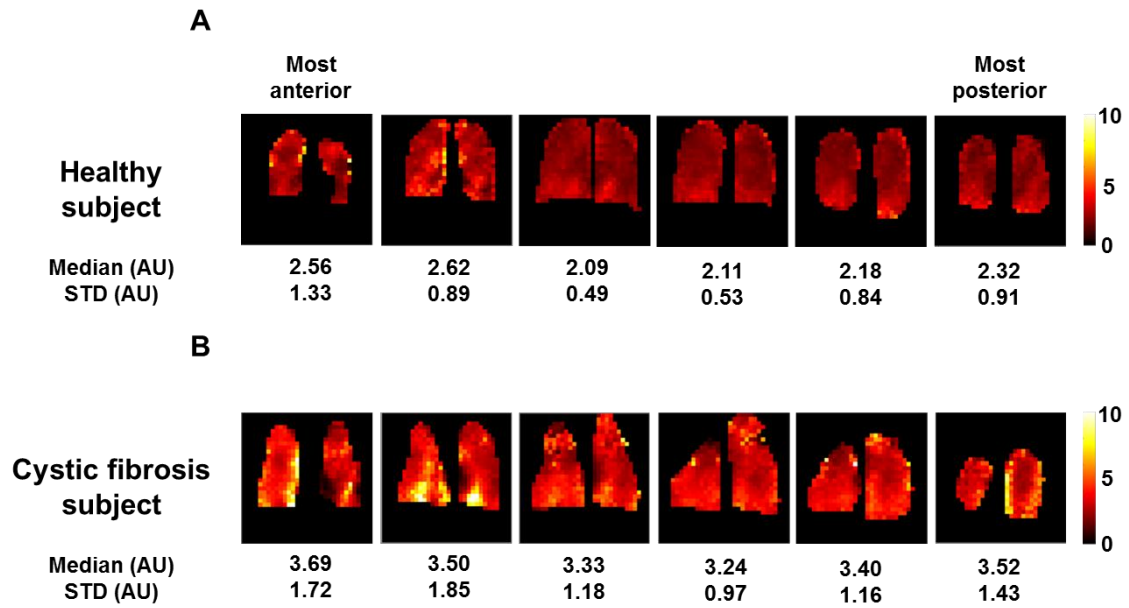


Figure 15 Coronal tissue/RBC ratio maps of a (A) healthy subject (subject 3) and (B) cystic fibrosis subject (subject 6) with respective median and standard deviation (STD) values. The CF subject presents a higher median and STD values for all slices in comparison with the healthy subject.

The ratios of the Xe-129 dissolved in tissue to that dissolved in the RBC for each slice of each subject as well as the mean ratios for each subject are depicted in Figure 16.

Subjects with the lowest predicted FEV₁ values (FEV₁ predicted of 55% and 71%) showed higher mean tissue/RBC ratio values (3.0 ± 0.36 , 3.4 ± 0.16 and 3.1 ± 0.34) in comparison with the healthy subjects (overall mean of 2.4 ± 0.22), with mean percentage differences of 25%, 42% and 29%.

The very mild-CF subject (FEV₁ predicted of 87%) presented a tissue/RBC ratio of 2.7 ± 0.27 , which is close to the healthy range. This result showed good agreement with the spirometry values, since they indicated an almost normal pulmonary function.

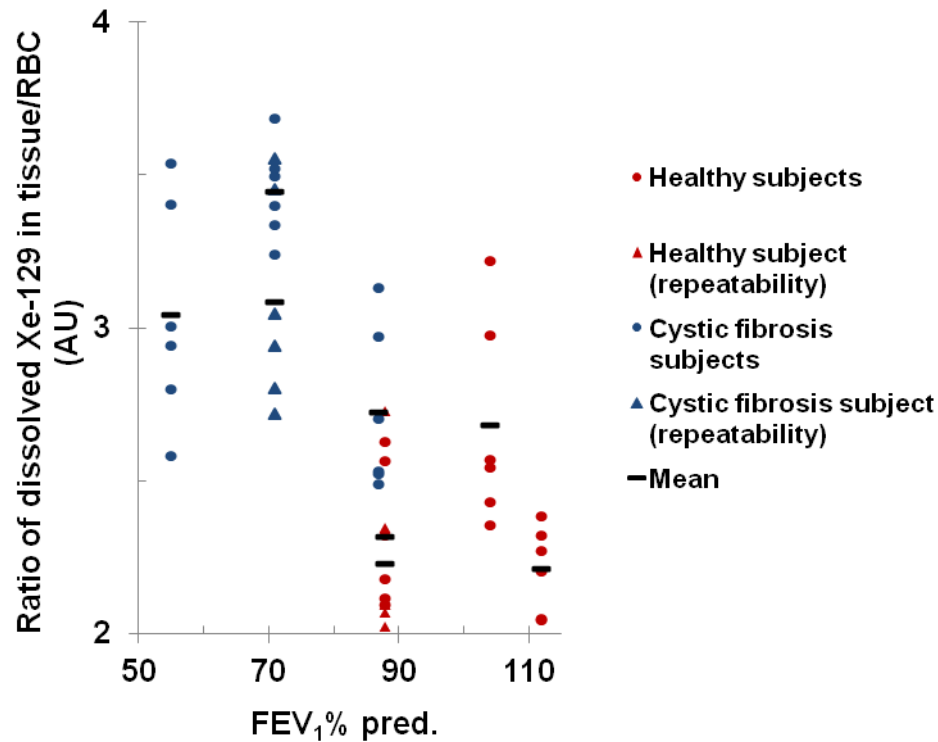


Figure 16 Quantification of the ratio of Xe-129 dissolved in tissue to that in RBC maps of all subjects, in arbitrary units (AU). Each point corresponds to a ratio value of one slice of each subject, whose pulmonary function is expressed by a spirometry measurement (percentage of predicted FEV₁). Subjects with the lowest predicted FEV₁ values presented higher tissue/RBC ratios.

For the two performed repeatability studies, the difference of the mean tissue/RBC ratios between the two consecutive acquisitions of the same subject was 10.5% for the CF subject (subject 6; FEV₁ predicted of 71%), and 3.9% for the healthy subject (subject 3; FEV₁ predicted of 88%).

2.4.2 Second-Hand Smoker subject

One SHS patient (subject 4) was added to this study to investigate if the 3D SB-CSI technique is sensitive to other respiratory diseases. In this case, the SHS presents spirometry values in the normal range (FEV₁ predicted of 94% and FEV₁/FVC of 0.76) and the gradient echo (GRE) ventilation images demonstrated a relatively homogenous gas distribution within the lung and throughout anterior to posterior slices (Figure 17A).

Regional Quantification of Lung Function in Cystic Fibrosis using hyperpolarized Xenon-129 and Chemical Shift Imaging

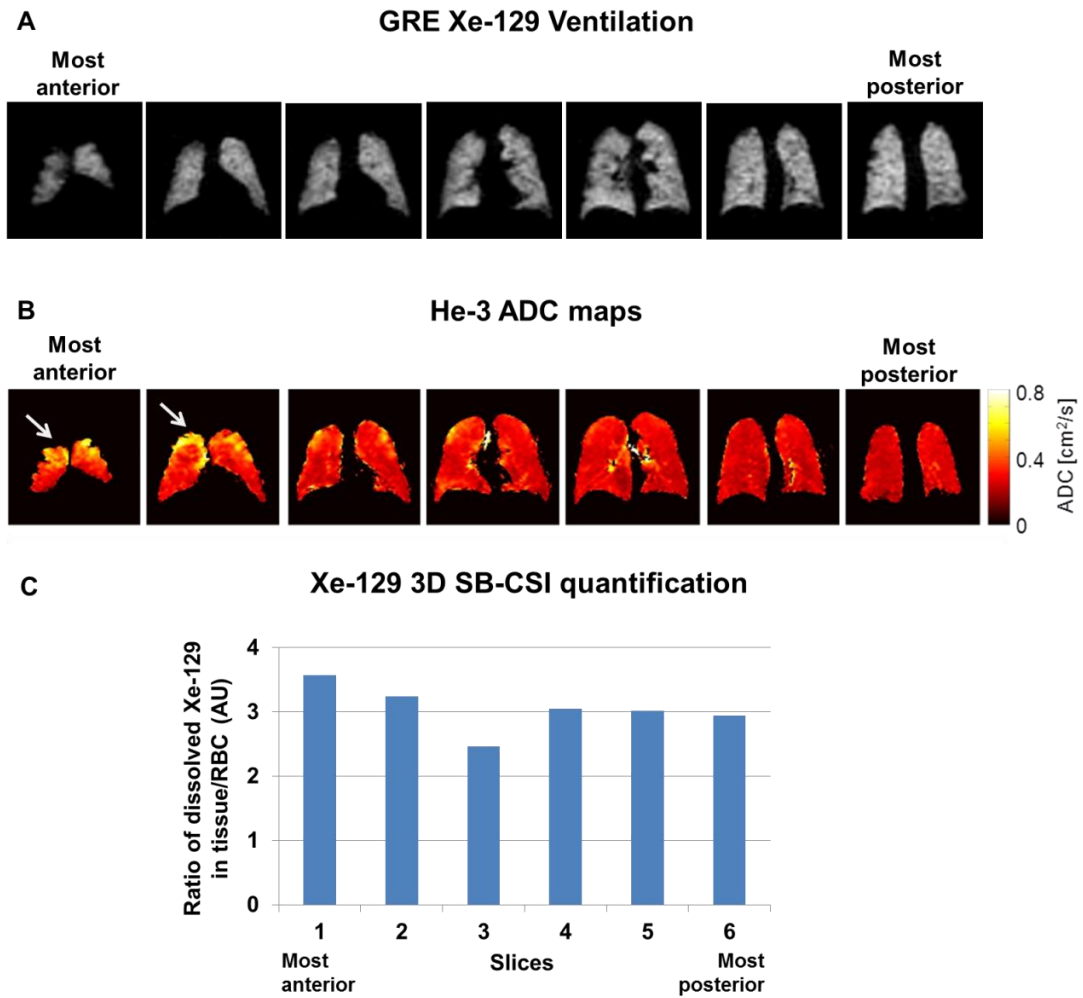


Figure 17 HP MR imaging lung measurements of the second-hand smoker subject (subject 4). (A) Ventilation maps obtained through a GRE sequence using Xe-129 as a contrast agent (TR 6.0 ms, TE 0.6 ms and in-plane resolution 7.5x7.5 mm²). (B) He-3 apparent diffusion coefficient (ADC) maps (TR 9.7 ms, TE 6.3 ms, in-plane resolution 3x3 mm² and b-values 0 and 1.6 s/cm²). (C) Quantification of Xe-129 CSI maps that express the amount of gas dissolved in tissue to that in RBC, in arbitrary units (AU). CSI quantification shows an increase in the tissue/RBC ratio most prominent in anterior slices, consistent with disease observed in He-3 ADC maps (white arrows).

However, a mean value of 3.0 ± 0.36 was obtained for the tissue/RBC ratio, which was similar to that obtained for the moderate-CF subject (3.0 ± 0.36). Moreover, the regional information provided by the tissue/RBC ratio of each slice (Figure 17C) demonstrated a higher incidence of disease in the most anterior slices. This was consistent with the focal elevations in the He-3 apparent coefficient diffusion (ADC) prominent most anteriorly (Figure 17B).

2.5 Discussion

As seen in the preliminary clinical data, healthy subjects presented uniform ventilation and gas uptake-exchange in the parenchyma and in the RBC, as expected.

This technique also detected a gradient from non-dependent (anterior) to dependent (posterior) regions of the lung. Since all subjects were imaged in the supine position, Xe-129 signal increase from anterior to posterior slices may be attributable to the gravity dependent lung effect, as seen elsewhere [12, 16, 35].

As predictable, the compression of the lung is more prominent in the gravitationally dependent portions, resulting in a higher tissue, alveoli and capillary density per unit volume of lung and thus increased amount of Xe-129 in those compartments. Gravity may also deform lung microstructure, producing smaller alveolar sizes, which results in higher alveolar surface-to-volume ratios in the dependent portion of the lung. The increase in this ratio should produce faster rates of transfer of Xe-129 into the tissue and blood. Gravitationally dependent gradients have also been detected through imaging of the HP He-3 ADC, which is sensitive to lung microstructure and consequently alveolar size [36].

Regarding the CF subjects, regions of deficient ventilation and gas uptake-exchange were visible within the lung. Structural abnormalities, such as bronchiectasis and inflammation of the bronchial walls, are thought to contribute to airflow obstruction in CF [30]. The fact that we were able to visualize regional abnormalities demonstrates that current resolution is sufficient to detect focal disease. In addition, the amount of defects in all lung compartment maps also appeared to be correlated with disease severity.

The lack of gradients from anterior to posterior slices was also detected in the moderate-CF subject. This suggests that the uptake-exchange of the gas is not uniform throughout the lung in cases of disease.

Most importantly, a lower and heterogeneous uptake-exchange of gas between the tissue and the RBC was observed in the CF population, demonstrated by higher values of median and STD of the tissue/RBC ratio. The increase in the ratio values of this population indicated that Xe-129 did not reach the RBC in the same time scale or quantity as occurred in healthy lungs, likely a result of the thickening of the parenchyma, caused by characteristic inflammation seen in CF disease [26].

Assessing the pulmonary wall thickness has proven to be a reliable method to distinguish healthy from diseased subjects. In fact, by calculating the tissue/RBC ratio, we were able to reveal disease in the SHS subject, not detected by the lack of sensitivity of the pulmonary function tests and functional information of ventilation images. This suggests that this method is very sensitive and may be able to provide additional information that could be useful for diagnosing and monitoring pathologies affecting the pulmonary uptake-exchange of gas, as when inflammation of lung parenchyma occurs. Since much of the research attention has focused on therapeutic anti-inflammatory strategies for the treatment of CF, the implementation of the 3D SB-CSI technique may be able to provide an earlier forecast of treatment response and outcomes.

This technique also proved to be able to achieve very reproducible results both in disease as well as in healthy subjects. The CF population was expected to be associated with higher errors since subjects with pulmonary diseases have difficulty in reproducing respiratory movements [26].

Conclusion

The preliminary results presented here let us hypothesize that the 3D SB-CSI technique may present improved sensitivity for the early detection and monitoring of several pulmonary diseases and conditions. Such method was able to generate ventilation maps that allowed assessment of gas distribution in the alveoli and correlated well with the existing imaging methods. Most importantly, 3D SB-CSI provided detailed 3D physiological information regarding gas uptake-exchange processes in a single and short breath-hold, capable of distinguishing healthy and diseased subjects.

The current version of the 3D SB-CSI technique takes about 15 s to acquire $18 \times 18 \times 8$ voxels, with an in-plane resolution of about $18 \times 18 \text{ mm}^2$. Further improvements, such as applying different techniques to reconstruct the maps, should provide additional temporal and spatial resolution, making this technique even more sensitive to small regional functional changes in the lung. The implementation of compressed-sensing data reconstruction methods may be capable of providing a significant acceleration by undersampling the data collected [37]. This could be important for the use of the 3D SB-CSI technique in pediatric population with CF or in other subjects with severe pulmonary disease that may not be able to hold their breath for large periods of time.

On the other hand, increased spectral resolution, in order to separate the tissue from the RBC peak, and thus measure precisely the fraction of Xe-129 dissolved in each compartment, would provide more sensitivity to this technique. According to Equation 4, the higher the magnetic field strength, the greater the separation in frequency of peaks will be. Therefore, a pilot study to determine whether 3 T is better suited for the 3D SB-CSI technique than the 1.5 T, would be appropriate.

Regarding the method chosen to analyze the data, a more automatic process would be desirable to reduce quantification time and errors associated with manual data manipulation. The pulse sequence used in this study has already been applied in multiple animal studies showing good results in terms of variability of phase offset within the lung [18-21]. Translating to greater lung sizes may potentiate a higher degree of magnetic field inhomogeneities that could be corrected with improvements in RF pulse design. Optimizing the RF pulse would also reduce the artifacts related with the vibration of the diaphragm depicted in the ventilation map of Figure 14 (white arrow). Furthermore, care

Regional Quantification of Lung Function in Cystic Fibrosis using hyperpolarized Xenon-129 and Chemical Shift Imaging

should be taken in order to maintain the same FA profile for all subjects, so that normalization with the gas peak would be sensitive to disease.

Finally, an exploratory study in a larger population is necessary to validate the results showed here. The results presented in this work may be used as guidance for future clinical studies using the 3D SB-CSI technique at the Department of Radiology and Medical Imaging of the University of Virginia. It is expected that in the next months more studies, focusing on CF disease as well as on chronic obstructive pulmonary disease, will be carried out there for validation of this technique.

References

1. van Echteld, C.J. and N. Beckmann, *A view on imaging in drug research and development for respiratory diseases*. J Pharmacol Exp Ther, 2011. **337**(2): p. 335-49.
2. Fain, S.B., et al., *Functional lung imaging using hyperpolarized gas MRI*. Journal of Magnetic Resonance Imaging, 2007. **25**(5): p. 910-23.
3. Kauczor, H., R. Surkau, and T. Roberts, *MRI using hyperpolarized noble gases*. Eur Radiol, 1998. **8**(5): p. 820-7.
4. Guenther, D., G. Hanisch, and H.U. Kauczor, *Functional MR imaging of pulmonary ventilation using hyperpolarized noble gases*. Acta Radiol, 2000. **41**(6): p. 519-28.
5. Albert, M.S., et al., *Biological magnetic resonance imaging using laser-polarized ^{129}Xe* . Nature, 1994. **370**(6486): p. 199-201.
6. Ruset, I.C., S. Ketel, and F.W. Hersman, *Optical pumping system design for large production of hyperpolarized Xe-129* . Phys Rev Lett, 2006. **96**(5).
7. Hersman, F.W., et al., *Large production system for hyperpolarized ^{129}Xe for human lung imaging studies*. Acad Radiol, 2008. **15**(6): p. 683-92.
8. Venkatesh, A.K., et al., *MRI of the lung gas-space at very low-field using hyperpolarized noble gases*. Magnetic Resonance Imaging, 2003. **21**(7): p. 773-776.
9. Sun, Y., et al., *Using hyperpolarized ^3He MRI to evaluate treatment efficacy in cystic fibrosis patients*. Journal of Magnetic Resonance Imaging, 2011. **34**(5): p. 1206-11.
10. Fain, S., et al., *Imaging of lung function using hyperpolarized helium-3 magnetic resonance imaging: Review of current and emerging translational methods and applications*. Journal of Magnetic Resonance Imaging, 2010. **32**(6): p. 1398-408.
11. Driehuys, B., et al., *Imaging alveolar-capillary gas transfer using hyperpolarized Xe-129 MRI*. Proceedings of the National Academy of Sciences of the United States of America, 2006. **103**(48): p. 18278-18283.
12. Cleveland, Z.I., et al., *Hyperpolarized (^{129}Xe) MR Imaging of Alveolar Gas Uptake in Humans*. Plos One, 2010. **5**(8).

13. Ruppert, K., et al., *Probing lung physiology with xenon polarization transfer contrast (XTC)*. Magnetic Resonance in Medicine, 2000. **44**(3): p. 349-57.
14. Ruppert, K., et al., *Exploring lung function with hyperpolarized (¹²⁹Xe) nuclear magnetic resonance*. Magnetic Resonance in Medicine, 2004. **51**(4): p. 676-87.
15. Ruppert, K., et al., *XTC MRI: sensitivity improvement through parameter optimization*. Magnetic Resonance in Medicine, 2007. **57**(6): p. 1099-109.
16. Mugler, J.P., et al., *Simultaneous magnetic resonance imaging of ventilation distribution and gas uptake in the human lung using hyperpolarized xenon-129*. Proceedings of the National Academy of Sciences of the United States of America, 2010. **107**(50): p. 21707-21712.
17. Swanson, S.D., et al., *Distribution and dynamics of laser-polarized (¹²⁹Xe) magnetization in vivo*. Magnetic Resonance in Medicine, 1999. **42**(6): p. 1137-45.
18. Mata, J., et al., *High-Resolution Chemical Shift Imaging of the Lungs with Xe-129 During a Single 6 Second Breath-Hold: Results from a Rabbit Model of Pulmonary Embolism*. Proceedings of the International Society of Magnetic Resonance in Medicine, 2008. **16**: p. 2679.
19. Mata, J., et al., *Chemical Shift Imaging of the lungs with hyperpolarized Xe-129: Results from a rabbit model of stereotactic lung radiosurgery with and without a radioprotector*. Proceedings of the International Society of Magnetic Resonance in Medicine, 2009. **17**: p. 2211.
20. Mata, J., et al., *Quantification and temporal study of physiologic lung changes in animal models of lung disease using 2D and 3D-CSI with Xe-129*. Proceedings of the International Society of Magnetic Resonance in Medicine, 2010. **18**: p. 989.
21. Mata, J., et al., *Improved Separation and Quantification of Xe-129 Dissolved-Phase Resonances in the Lung*. Proceedings of the International Society of Magnetic Resonance in Medicine, 2011. **19**: p. 884.
22. Bernstein, M.A., K. F. King and X. J. Zhou, *Handbook of MRI pulse sequences*, 2004: Elsevier Academic Press.
23. Nagashima, K., *Optimum pulse flip angles for multi-scan acquisition of hyperpolarized NMR and MRI*. J Magn Reson, 2008. **190**(2): p. 183-8.
24. Eichinger, M., et al., *Morphologic and functional scoring of cystic fibrosis lung disease using MRI*. Eur J Radiol, 2011.

25. Foundation, C.F. *About Cystic fibrosis*. 2012; Available from: <http://www.cff.org/AboutCF/>.
26. Davies, J.C. and E.W. Alton, *Monitoring respiratory disease severity in cystic fibrosis*. *Respir Care*, 2009. **54**(5): p. 606-17.
27. Inc., V.P. *Kalydeco (ivacaftor) tablets*. 2012; Available from: <http://www.kalydeco.com/>.
28. Altes, T.A., M. Eichinger, and M. Puderbach, *Magnetic resonance imaging of the lung in cystic fibrosis*. *Proc Am Thorac Soc*, 2007. **4**(4): p. 321-7.
29. Kerem, E., et al., *Prediction of mortality in patients with cystic fibrosis*. *N Engl J Med*, 1992. **326**(18): p. 1187-91.
30. Tiddens, H.A., et al., *Cartilaginous airway wall dimensions and airway resistance in cystic fibrosis lungs*. *Eur Respir J*, 2000. **15**(4): p. 735-42.
31. Keeler, J., *Understanding NMR Spectroscopy*, 2005: John Wiley & Sons Ltd.
32. Grandinetti, P.J., *Nuclear Magnetic Resonance for people*, 2011.
33. Facility, U.o.O.N. *The Phase of an NMR Spectrum*. 2012; Available from: <http://u-of-o-nmr-facility.blogspot.com/2010/11/phase-of-nmr-spectrum.html>.
34. Stoyanova, R. and T.R. Brown, *NMR spectral quantitation by principal component analysis. III. A generalized procedure for determination of lineshape variations*. *J Magn Reson*, 2002. **154**(2): p. 163-75.
35. Prisk, G.K., et al., *Pulmonary perfusion in the prone and supine postures in the normal human lung*. *J Appl Physiol*, 2007. **103**(3): p. 883-94.
36. Fichele, S., et al., *MRI of helium-3 gas in healthy lungs: posture related variations of alveolar size*. *Journal of Magnetic Resonance Imaging*, 2004. **20**(2): p. 331-5.
37. Lustig, M., D. Donoho, and J.M. Pauly, *Sparse MRI: The application of compressed sensing for rapid MR imaging*. *Magnetic Resonance in Medicine*, 2007. **58**(6): p. 1182-1195.